Aus dem Institut für Schlaganfall- und Demenz Forschung
Institut der Ludwig-Maximilians-Universität München
Vorstand: Prof. Dr. Martin Dichgans

Functional connectivity analysis in health and brain disease using in vivo widefield calcium imaging

Dissertation
zum Erwerb des Doktorgrades der Medizin
an der Medizinischen Fakultät der
Ludwig-Maximilians-Universität zu München

vorgelegt von
Julia Verena Cramer

aus
München

2020

Mit Genehmigung der Medizinischen Fakultät
der Universität München

Berichterstatter:	PD Dr. med. Arthur Liesz
Mitberichterstatter:	Prof. Dr. Sibylle Ziegler Priv. Doz. Dr. Monika Bradl Priv. Doz. Dr. Phillipp Kazmierczak
Mitbetreuung durch den promovierten Mitarbeiter:	
Dekan:	Prof. Dr. med. dent. Reinhard Hickel
Tag der mündlichen Prüfung:	03.12.2020

Für

Mama und Toni

AFFIDAVIT

Cramer, Julia Verena

Name, Vorname

Ich erkläre hiermit an Eides statt,

dass ich die vorliegende Dissertation mit dem Thema

“Functional connectivity analysis in health and brain disease using *in vivo* widefield calcium imaging”

selbstständig verfasst, mich außer der angegebenen keiner weiteren Hilfsmittel bedient und alle Erkenntnisse, die aus dem Schrifttum ganz oder annähernd übernommen sind, als solche kenntlich gemacht und nach Herkunft unter Bezeichnung der Fundstelle einzeln nachgewiesen habe.

Ich erkläre des Weiteren, dass die hier vorgelegte Dissertation nicht in gleicher oder in ähnlicher Form bei einer anderen Stelle zur Erlangung eines akademischen Grades eingereicht wurde.

München, 10.12.2019 — Julia Verena Cramer

Ort, Datum — Julia Verena Cramer

Table of contents

1 Introduction

> *If the human brain were so simple that we could understand it, we would be so simple that we couldn't.*
>
> Emerson W. Pugh, The Biological Origin of Human Values

The brain's complexity is still challenging, fascinating and inspiring for thousands of scientists worldwide. The history of neuroscience is characterized by the investigation of famous patients such as Phineas Gorge, Kent Crochane and Henry Molaison. What do most these patients have in common? For various reasons the structural integrity of their brains suffered greater damage. And all of them presented striking deficits. At the expense of their fate, neuroscience research gained immense insight on functions attributed to specific brain regions. This knowledge surely played a major role in starting to understand complex brain functions in general. However, the more the understanding of the brain evolves the more complex it appears. And unfortunately, until now all the gained knowledge only very marginally helped those patients which suffered structural brain damage such as traumatic brain injury or stroke. What is hindering modern neuroscience to help the very people whose fate advanced our knowledge so much? And are there possibilities to change this? We will see some obstacles imposed in modern stroke research and one way to improve it to hopefully give back the knowledge to these patients.

1.1 Stroke

Stroke is an acute cerebrovascular disease and defined by the World Health Organisation (WHO) as following:

"A stroke is caused by the interruption of the blood supply to the brain, usually because a blood vessel bursts or is blocked by a clot. This cuts off the supply of oxygen and nutrients, causing damage to the brain tissue. The most common symptom of a stroke is sudden weakness or numbness of the face, arm or leg, most often on one side of the body. Other symptoms include: confusion, difficulty speaking or understanding speech; difficulty seeing with one or both eyes; difficulty walking, dizziness, loss of balance or coordination; severe headache with no known cause; fainting or unconsciousness. The effects of a stroke depend on which part of the brain is injured and how severely it is affected. A very severe stroke can cause sudden death."[1]

1.1.1 Epidemiology

According to the World Health Organisation's (WHO) report from 2016, stroke is the second most common cause of death worldwide[2]. About 5.5 million deaths were accounted to cerebrovascular disease and about half of them to ischemic stroke[3]. In 2016, prevalence of total cerebrovascular disease was estimated to be 79.6 million worldwide, whereof 67.6 million patients suffered from ischemic stroke[3,4]. Globally, the prevalence of stroke is predicted to further increase due to aging of the population[3,5–7]. The consequences of stroke can range from minor deficits such as subtle motoric weakness over loss of independency in daily activities to serious long-term disability with extensive nursing care needs. In the United States stroke is among the 10 most common causes of long-term disability[8]. Here again, the number of disability-adjusted life-years (DALY) —a measure to quantify burden of disease— significantly increased from 1990 to 2013 worldwide[9]. In fact in 2013, stroke was the second most prominent contributor to DALY with 113 million years lost[9]. Stroke has additionally a large impact on economy. The costs of stroke in Europe were estimated to be €45 billion a year. This economic burden can be divided in direct health care costs (€20 billion) spent on in-hospital care and drugs, and additional non-health care costs which arise through productivity loss (€9 billion) and the informal care of people with stroke (€16 billion)[10]. Consequently, more than half of the costs can be accounted by the long-term consequences of stroke. Hence, chronic disability after stroke has the highest impact on both the individual quality of life and the social-economic system.

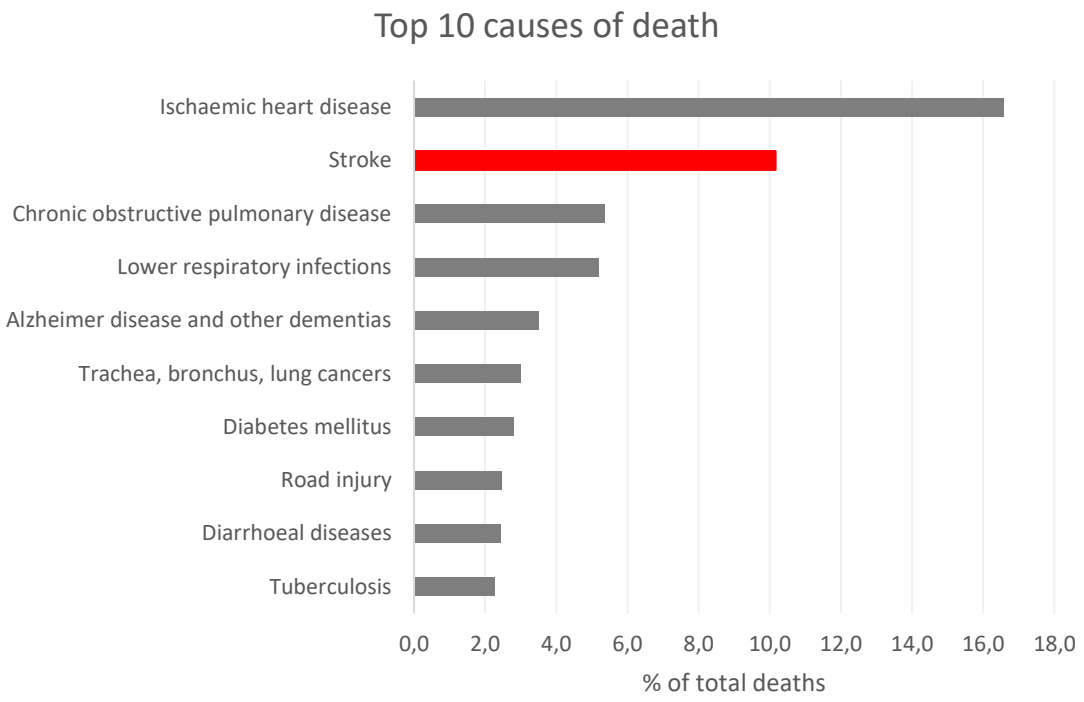

***Figure 1: Top 10 causes of death worldwide**. With 10.5% stroke is the second leading cause of death worldwide in 2016. Epidemiological data origins from Global Health Estimates 2016: Deaths by Cause, Age, Sex, by Country and by Region, 2000-2016. Geneva, World Health Organization; 2018*[11].

1.1.2 Pathophysiology

Stroke is a vascular disease. The pathophysiology of stroke can be divided in two major sub-types: cerebral ischemia and cerebral haemorrhage[12]. Cerebral haemorrhage, often referred to as primary haemorrhagic stroke, is characterized by the rupture a blood-vessel and subsequent extravasation of blood. The localisation of the ruptured vessel can differ and divide further subtypes. With about 10% haemorrhagic stroke is less common than ischemic stroke (circa 87%)[3]. Ischemic stroke can be caused by various conditions and results in an occlusion of a cerebral artery either by embolism or thrombosis. Among all underlying conditions, the three leading causes are cardioembolism, macroangiopathy e.g. atherosclerosis of the arteria carotis interna and microangiopathy promoted by diabetes mellitus and high blood pressure[13]. Those three conditions are responsible for around 70% of all ischemic strokes[14,15]. Pathophysiologically, ischemic stroke is characterized by oxygen and glucose restriction due to impaired blood flow resulting in brain tissue necrosis in the area of the supplying artery. The brain tissue receiving supply by the occluded vessel undergoes several phases before final permanent necrosis. In general, brain tissue permanently relies on oxygen and glucose supply by cerebral arteries. If this supply comes below a certain threshold functional metabolism cannot be maintained and neurological symptoms appear. If the supply continues to fall, structure metabolism stops and tissue undergoes permanent necrosis which constitutes the core of the infarct[16,17]. This area is often surrounded by tissue at risk which is already affected but its structure metabolism is still maintained[17]. Existing therapeutic strategies of ischemic stroke aim to rescue the tissue at risk to reduce necrotic brain area and with this the extension of neurologic deficits.

1.1.3 Therapeutic strategies of ischemic stroke

Despite the huge socio-economic burden of stroke there is only few therapeutic options for ischemic stroke. In the very acute phase, the aim of therapy is the removal of the thrombus occluding the vessel. Today, there is only two clinically approved therapies for acute ischemic stroke: Thrombolysis with tissue plasminogen activator (tPA) and thrombectomy via mechanical vascular recanalization[18,19]. To guarantee safety of both therapies stringent requirements must be fulfilled. Both strategies have to be applied within a narrow time window shortly after stroke onset to maximize their benefit: within 4.5 hours for thrombolysis and 6 hours (up to 24 hours) for thrombectomy[18]. Besides this temporal limitation, various additional conditions such as presumed very-large infarction, intracranial haemorrhage, coagulation abnormalities and several others contradict these approaches[18,20]. Though being very effective, only about 10% of patients who suffer from acute ischemic stroke and are admitted to hospital receive intravenous thrombolysis[21]. Following the acute phase, secondary prevention aims to reduce the risk of secondary events by diminishing cardiovascular risk factors. Besides lifestyle changes both pharmacological and operative strategies are available, depending on the primary cause leading to stroke. Carotid endarterectomy can be considered if stenosis of the carotid artery is the underlying cause and anticoagulants if a cardioembolic cause is assumed[18,20]. Antiplatelet drugs and statins are provided to reduce cardiovascular risk[18,20]. Today, the only known

regenerative treatment is rehabilitation which stroke survivors receive early after stroke to improve their quality of life and to rise the number of self-sufficient persons[18]. Overall, therapeutic options for patients suffering from stroke remain poor. Hence, new effective strategies are urgently sought for given the increasing number of patients in the ageing population in future. Although more than thousand neuroprotective drugs have been established in preclinical experiments, none of them proved efficacy in clinical trials[22,23]. What is the reason the biological effect becomes lost in translation? It is discussed that especially animal models, the way drugs are applied, blinding throughout the experiment and publication bias contribute to this concerning circumstance[24–26]. In general, all the named arguments impede the comparability of preclinical and clinical trials. But there are additional parameters which lately gain more and more attention[27]. One of them is the lack in comparable assessments to monitor the outcome in preclinical studies. Especially, to investigate long-term recovery, translational methods to assess functional outcome are indispensable[27]. In preclinical trials, functional outcome is most frequently assessed via behaviour tests. Those however are very vulnerable to subjective bias, are time consuming and inconsistent protocols impair comparability between laboratories[28,29]. Hence, with only behaviour testing there is a lack of translational readouts in preclinical studies which urgently needs to be filled. In search for bridging this gap one can orientate on clinical research. There, one of the most promising methods for successful translation to preclinical research is functional imaging. Functional imaging allows to monitor brain activity and with this one functional readout. With functional imaging in preclinical research objective functional endpoints can be acquired, a deeper understanding of possible pathomechanisms achieved and findings compared and translated to clinical research[27]. Additionally, functional imaging offers the possibility of future potential prognostic values[30]. As a widely used method in human research, functional imaging is one option to bridge the translational gap and might be crucial to promote new therapies from experimental research to effective human stroke treatment.

1.2 Functional imaging

Functional imaging in general is an imaging technique to detect and assess physiological processes such as alterations in blood flow, absorption, metabolism and others. In contrast to structural imaging, its main aim is to characterize and investigate the physiology of a defined organ within the body. In order to do so, special imaging techniques combined with a specific indicator are used to map activity both spatially and temporally. The indicators are chosen in such a way as to play a key role within the investigated process. In neuroscience, the most widely used method to acquire functional imaging data is functional magnetic resonance imaging (fMRI)[31,32]. fMRI is commonly used to study brain activity in both health and disease to better understand physiological and pathophysiological changes in humans. However, new therapeutic targets are mostly developed in small animal models, most commonly mice. To bridge translational gaps, functional imaging of brain activity should be made available for small rodents as it can provide crucial insight into the impact of novel therapeutic

strategies on pathophysiological mechanisms in brain diseases. Due to several reasons, acquisition of fMRI in mice is often not a feasible option. Briefly, in fMRI, cerebral blood flow and more specifically its oxygenation status are measured. This is possible since oxygenated blood is less magnetic (diamagnetic) whereas deoxygenated blood is more magnetic (paramagnetic) and consequently oxygenated blood disturbs the magnetic field less than deoxygenated[31]. This blood-oxygen-level-dependent (BOLD) effect can be detected by the MRI non-invasively and is believed to reflect neural activity[33,34]. The premise to draw conclusions from blood flow about brain activity is known as neurovascular coupling: A phenomenon characterized by a high correlation between blood-flow and neural activity in the healthy brain[33]. Hence, fMRI measures brain activity indirectly with the BOLD effect as its surrogate parameter. Even though fMRI is a very well-established method in humans, obtaining fMRI in mice is very challenging. Since acquiring the MRI sequences take long time, fMRI recording usually goes in hand with the need for deep and long anaesthesia for the animals. Additionally, resolution of the images in relation to the mouse body is very low and this modality is very time- and cost-intensive. All these challenges reveal the need for an alternative method which allows the analysis of functional imaging in mice. Among different options we decided to refine the protocol for the analysis of functional imaging in mice expressing a calcium sensor in excitatory neurons: *in vivo* widefield calcium imaging of both cerebral hemispheres.

1.2.1 *In vivo* widefield calcium imaging

In vivo widefield calcium imaging is a relatively new method to assess brain activity in mice. The underlying principle is the fluctuation of intracellular calcium concentration during the action potential. Those calcium transients can be used and made visible with calcium sensitive dies. Sabatini et al. demonstrated a strong correlation between experimentally induced action potentials and intensity changes of one of those calcium sensitive fluorophores[35] (**Figure 2**).

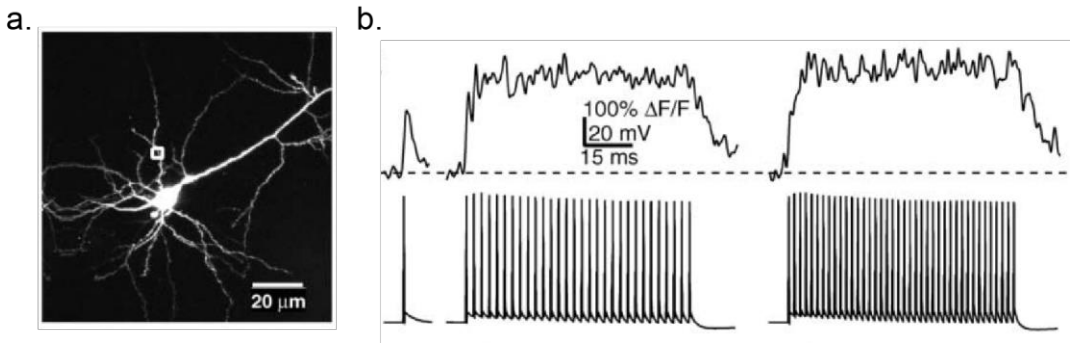

Figure 2: Action potential-evoked calcium fluctuations in dendrites and spines. a. *Image of a CA1 pyramidal neuron loaded with a green calcium sensor (Fluo-4).* ***b.*** *Changes in green fluorescence intensity a single action potential (left) or by trains at 62.5 (middle) or 83.3 (right) Hz (average of 15, 4, and 4 trials, respectively) measured with a custom-built two-photon laser scanning microscope. Intracellular Calcium-driven changes in fluorescence correlate with neural activity. Modified from Sabatini et al. with permission*[35].

For *in vivo* widefield calcium imaging, we used a transgenic animal expressing a genetically encoded calcium indicator (GECI) in neurons. In these animals, neural activity can be assessed directly via changes in the fluorophore's intensity. In particular, we used Thy1-GCamP6s heterozygous mice, which express a green fluorescent protein (GFP) bound to calmodulin protein (CaM) termed GCaMP. In Thy1-GCaMP mice the GECI is expressed under the neuronal Thy1 promotor and hence predominantly present in layer 5 but also layer 2 and 3 pyramidal cells[36]. CaM is a calcium binding protein which senses alterations in calcium levels during neural activity. In presence of calcium, the GCaMP protein changes conformation and as a consequence alters the spectral properties of the chromophore[37,38]. The alterations in fluorescence can be optically recorded. It is well investigated, that changes in intensity of emitted GFP signal mirror neural activity in these transgenic animals[39,40].

The most common application for these transgenic animals is two-photon imaging. This imaging method allows to assess single cell activity and the characterization of microscale networks. A novel approach however is to assess entire cortical information: *in vivo* widefield calcium imaging. Here, cortical neural activity of the entire forebrain can be monitored in real time by acquiring intensity changes of GCaMP fluorescence via a highly sensitive camera. We evolved this method with a stringent experimental protocol and appropriate analysis strategies to create a truly translational tool. To maximize comparability to human functional imaging, we established protocols for the most common imaging paradigms.

1.2.2 Imaging paradigms

Classically, two different experimental settings are defined: task dependent and resting state imaging paradigm. In task dependent imaging, brain activity is assessed while a task is performed. This can be a cognitive or motoric task *sensu stricto* or some sort of sensory or acoustic stimulation. Areas of the brain processing this information will be specifically activated and can be interpreted as a small network. In this work we performed sensory stimulation of all four paws of the animal. To underline this passive stimulation, we termed our experimental set-up as stimulus dependent imaging. In contrast to task dependent imaging, resting state imaging demands no specific task. Image acquisition is performed while external input is diminished, e.g. no task is presented, and intrinsic brain activity is recorded. In resting state brain imaging, one major readout is functional connectivity which is characterized as synchronicity of brain activity in spatially distinct areas and obtained by Pearson's correlation r of the signal time series[41,42]. Functional connectivity is defined higher with higher correlation of the signal time series and hence goes in line with the Hebbian theory "What fires together, wires together". Even though the protocols of both task dependent and resting state paradigm are quite contrary their results can be viewed as complementary: There is consensus, that networks revealed during task dependent imaging resemble those which show intrinsic functional connectivity assessed during resting state imaging in humans[34,43]. Hence, we established both paradigms in order to fully characterize functional cortical networks in the healthy mouse first. Consequently, we

investigated the alterations in functional connectivity due to brain disease in an experimental stroke model.

1.3 Aims of this study

The aim of this work was to establish an imaging method which allows for comparison of preclinical and clinical research results and with this to bridge the gap in between them. To achieve this aim, we needed to ensure three qualities: the method needed to be reproducible, functional and translational. These qualities were approached by three different experimental studies. In the anaesthesia study we investigated the impact of anaesthesia on brain activity and functional connectivity. Consequently, we established a stringent experimental and analytical protocol to diminish its influence on the data and raise reproducibility. Then, to guarantee functionality we performed the network study. Here, we identified independent cortical areas via independent vector analysis (IVA) and assigned them physiological function via stimulation. Lastly, in the stroke study we implemented our novel tool to investigate brain disease. We characterized the impact of cortical stroke in the motor area on functional brain activity in both acute and chronic phase. This third study was meant to demonstrate our tool being translational.

2 Materials and Methods

2.1 Materials

2.1.1 Equipment

PRODUCT NAME	COMPANY
Equipment for *in vivo* methods	
PeriCam PSI System	Perimed, Sweden
Stereotakctic frame (product no.: 51501)	Stoelting, Europe
Vaporizers ASA Isoflurane	Harvard Apparatus, USA
DigiFlow 3 l/min	Dräger, Germany
Navigator Scale	OHAUS, USA
Induction chamber	Werkstatt
Tubes	Werkstatt
Laser Cobolt HS-03	Solna, Sweden
Cobolt Jive 50 561 nm	Solna, Sweden
Fiber Collimation Package F240APC-A	Thorlabs, USA
Laser eyewear Laser 2000	Scitec instruments, United Kingdom
Multimark 1523 permanent	Faber-Castell, Germany
Timer Product Number TR118	Oregon scientific, USA
Disposable Scalpel	Feather Savety Razor, Japan
Scissors Prod Number: 14090-11	Fine Science Tools, Dumont, Switzerland
Forceps Prod Number: 91197-00	Fine Science Tools, Dumont, Switzerland
Heating chambers MediHeat	Peco Services Ltd, United Kingdom
DC Temperature Controller	FHC, USA
HC V380 Camcorder	Panasonic, Japan
Wooden Beams (100.0x2.0x0.5 cm)	Obi, Germany
Plattform	Obi, Germany
Equipment for the imager	
Imager 3001	Optical Imaging Ltd, Israel
SOLIS 445B/M	Thorlabs, USA
Advanced Solis LED Driver DC2200	Thorlabs, USA
515 nm longpass filter	Optical Imaging Ltd, Israel
495 nm dichroic longpass filter	Optical Imaging Ltd, Israel
NIKKOR 85 mm f1.4	Nikon, Japan
NIKKOR 50 mm f1.2	Nikon, Japan
Adimec 1000-m/D	Adimec, Netherlands

DG2A	Digitimer Ltd, UK
DS3	Digitimer Ltd, UK
Acupuncture needles	Hwato, China
MLA 1204 Needle Electrodes	ADInstruments, New Zealand
Adapter (Product number 610248)	Ternimed, Germany
PowerLab 16/35, ADInstruments, New Zealand	ADInstruments, New Zealand
Equipment for in vitro methods	
Research Plus Pipette	Eppendorf, Germany
Acculab Analytical Balance ALC – 80.4	ACCULAB sartorius group, Germany
PH Meter Lab 855	SI Analytics, Germany

2.1.2 Consumables

PRODUCT NAME	COMPANY
Coverslips (24x60mm #1,5)	Menzel-Gläser, Germany
Superfrost Plus Microscope Slides	Menzel-Gläser, Thermoscientific, Germany
Vasco Nitril Blue Gloves	Braun, Germany
Quick Base S398	Parkell C&B metabond, USA
L-Powder clear S399	Parkell C&B metabond, USA
Universal Catalyst S371	Parkell C&B metabond, USA
Bepanthen eye cream	Bayer AG, Germany
PP-Overall	Falano, Germany
Barrier Surgical hood REF 42072	Mölnlycke health care, Australia
Medical face Maskv REF 657010	Mölnlycke health care, Australia
Injekt 5 ml	Braun, Germany
Microlance Needles 27Gx ¾“ – Nr. 20	BD, Becton, Spain
Cotton applicator	NOBAMED PaulDanzAG, Germany
Mikrozid AF wipes disinfection	Schülke, Germany
Surflo winged infusion set with protector	Terumo, Belgium
Colour Coding Dots	Avery Dennison Zweckform Office Products Europe GmbH, Germany
Kimtech Science Precision Wipes	Kimberly-Clark Professional, United Kingdom

2.1.3 Chemicals

PRODUCT NAME	COMPANY
Isoflurane Iso-Vet 1000mg/g	Dechra, Germany
0.9% NaCl	Berlin-Chemie AG, Germany

Ketamin 10%	Medistar, Germany
Xylanin 20mg/ml	WTD, Germany
Medetomidin (Dorbene vet 1mg/ml)	Zoetis, Germany
Atipamezol (Atipam 5mg/ml)	Dechra, Germany
Carprofen (Rimydyl 50ml/ml)	Zoetis, Germany
Rose Bengal	Sigma-Aldrich, USA
Octenisept	Schülke, Germany
Calcium chloride	Sigma-Aldrich, USA

2.1.4 Software

SOFTWARE NAME	COMPANY
MATLAB R2016b	The MathWorks, USA)
longDaq	Optical Imaging Ltd, Israel
VDaq	Optical Imaging Ltd, Israel
LabChart	ADInstruments, New Zealand
PIMSoft Version 1.2.2.0	Perimed, Sweden
ImageJ, Version 1.49c	Fiji, USA
GraphPad Prism Version 6.0	GraphPad Software, USA

2.2 Methods

2.2.1 Three step study design: the anaesthesia, the network and the stroke study

We conducted three sub-studies in order to establish *in vivo* widefield calcium imaging. In the first study –the anaesthesia study— we investigated the effect of anaesthesia on functional imaging. Therefore, we evaluated three different anaesthesia protocols (1.5% ISO, 1.0% ISO, MED+ISO; n=9). The protocol resulting in the lowest anaesthesia depth possible while achieving consistent imaging quality across animals and days was used in the remaining two studies.

In a second step –the network study— we aimed to define functional relevant cortical areas. We used an independent component analysis (ICA) on resting state data (n=41-47) to identify functional networks within the cortex. We evaluated the functional contribution of the identified cortical network components by somatosensory stimulation (n=23). We further defined regions of interest (ROI) centred around the peak pixel of the areas being part of the independent component spatial maps.

In the final stroke study, we investigated the changes in functional connectivity after ischemic stroke. We implemented both the established anaesthesia protocol and ROI to evaluate the pathological changes and the recovery process after an acute injury to the motor cortex (sham n=17; stroke n=23). The stroke study was performed with in total 7 subgroups of mice, from which all were followed up

until day 28 and only the final two groups until day 56 after stroke. Additionally, the stroke study aimed to support the concept that *in vivo* widefield calcium imaging together with an advanced analysis pipeline a valuable tool in the study of disease models.

2.2.2 *In vivo* experiments

2.2.2.1 Animals

All experiments were conducted in accordance with national guidelines for the use of experimental animals and all protocols were approved by the German governmental committees (Regierung von Oberbayern, Munich, Germany). Mice were held at regulated temperature (22 ± 2 °C), with a 12-h light–dark cycle period. They had access to food and water *ad libitum*. Throughout all anesthetized procedures body temperature was sustained using a feedback-controlled heating system and the eyes were moisturized using Bepanthen ointment (Bayer, Germany). Until full recovery from anaesthesia, animals were placed into a heating chamber.

2.2.2.1.1 Mouse strain

C57BL/6J-Tg(Thy1-GCaMP6s)GP4.12Dkim/J[36] heterozygous mice (Thy1-GCaMP) were bred at the Institute for Stroke and Dementia Research, Munich. In these animals GCaMP expression is regulated by the Thy1 promoter and therefore restricted specifically to excitatory neurons, predominantly layer 5 as well as layer 2 and 3 pyramidal cells (**Figure 3**).

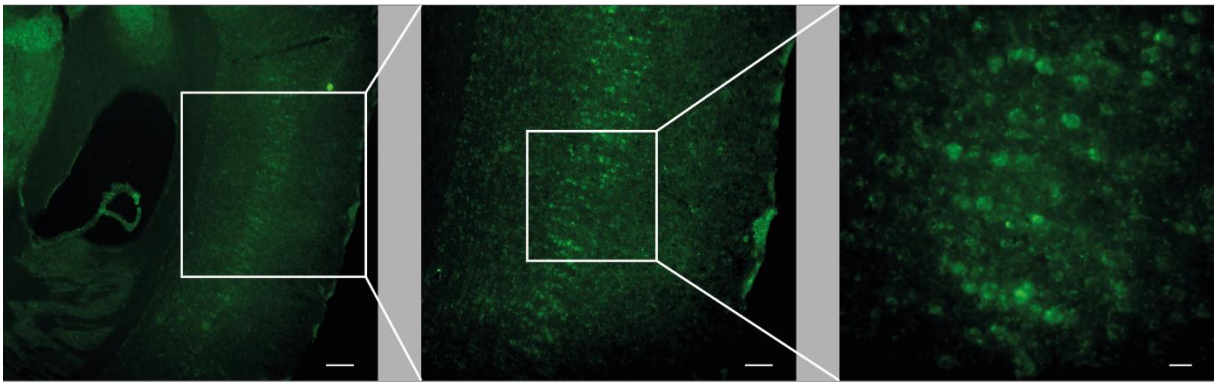

Figure 3: Histological analysis of cortical expression pattern of GCaMP protein in Thy1-GCaMP6s heterozygous mice. *Green fluorescence reveals predominant expression of GCaMP protein in layer 5 as well as 2 and 3. Epifluorescence pictures with 5x, 10x and 40x magnification. Scale indicates 200 µm, 100µm and 20 µm respectively.*

2.2.2.1.2 Sex and age of the mice

This study included mice of both sex at 12-15 weeks of age. As animals underwent skull preparation in order to enable *in vivo* widefield calcium imaging, growth of the skull had to be sufficiently completed. The age of 12-15weeks was evaluated to be the best due to full-grown size of the skull.

2.2.2.2 *In vivo* widefield calcium imaging

The protocol of *in vivo* widefield calcium imaging consists of several sub steps. As an overview, firstly the skull of the animals was prepared with a chronic ‘window’ couple of days before the first

acquisition. Animals were allowed full recovery for several days before the first imaging acquisition. For each acquisition, mice were anesthetized and placed in the stereotactic frame below a customized imaging set-up. Depending on the experimental design only resting state imaging was performed or in a subgroup of animals additional stimulus-evoked brain activity was recorded. After anaesthesia, animals were kept in a heating chamber at 37°C until full recovery. All sub steps such as skull preparation, imaging set-up, anaesthesia protocol and imaging paradigm themselves will be explained in the following paragraphs.

2.2.2.2.1 Animal preparation

Skull preparation was performed using a modified version of the previously published protocol of Silasi et al.[44]: First, animals were anesthetized using 5% isoflurane for induction and 2% isoflurane for maintenance vaporized in 30% O_2 and 70% N_2O. After induction, animals were placed into a stereotactic frame (product no.: 51501, Stoelting, Europe) fixing the animal's head to generate stable surgery conditions. After disinfection, the head was carefully scalped, and the underlying connective tissue was gently removed whilst the skull stayed fully intact. The exposed intact skull was cleaned, disinfected and led dry. In the meantime, a three-component transparent dental cement (Quick Base S398, L-Powder clear S399 and Universal Catalyst S371, Parkell C&B metabond, USA) was mixed. A thin layer was applied upon the intact skull and covered immediately with a tailored coverslip (24x60mm #1,5, Menzel-Gläser, Germany). The mice stayed anesthetized until the cement was fully dried and could recover at least 48h before the first image acquisition. Two mice (one in stroke, one in sham group) removed their cranial windows (after 5 and 42 days respectively) and were consequently excluded from further recordings.

2.2.2.2.2 Set up

The imaging set-up consisted of the following products (**Figure 4**):

- a blue light emitting diodes (LED) lamp with 445nm nominal wavelength with 23 nm bandwidth (SOLIS 445B/M, Thorlabs, USA)
- a constant current generator (Advanced Solis LED Driver, Thorlabs, USA)
- a 495 nm dichroic longpass filter (Optical Imaging Ltd, Israel)
- a 515 nm longpass filter (Optical Imaging Ltd, Israel)
- two video lenses (NIKKOR, 85 mm f1.4, and NIKKOR 50 mm f1.2; Nikon, Japan)
- a 2/3″ Interline CCD camera with 7.4 x7.4 μm pixel size (Adimec 1000-m/D, Adimec, Netherlands)
- Imager 3001 (Optical Imaging Ltd, Israel)
- a customized longDaq software (Optical Imaging Ltd, Israel)

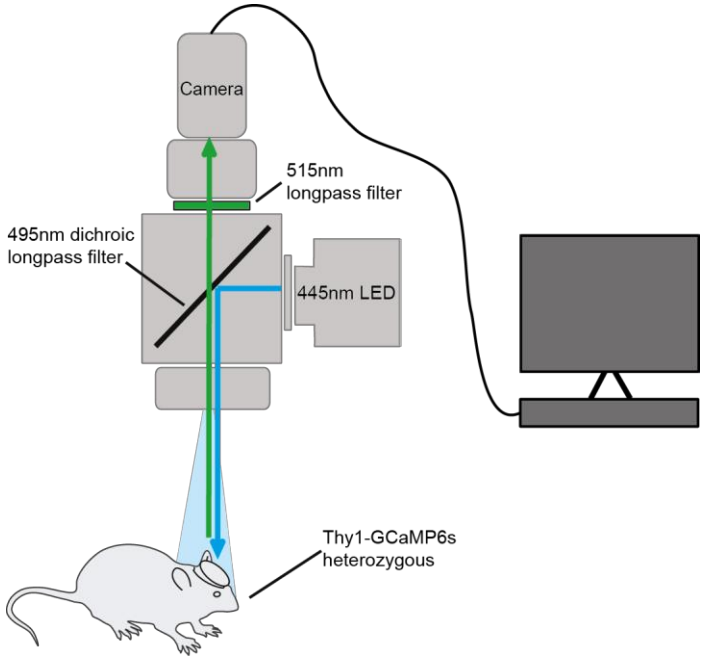

Figure 4: Scheme of the customized imaging set-up. *A 450nm LED light beam (blue arrow) was redirected by a dichroic longpass filter into the optical path to illuminate the cortex of the Thy1-GCaMP6s heterozygous mouse to excite the GCaMP protein expressed in pyramidal cells. The emitted GFP fluorescence (green arrow) passed back through two lenses and a 515nm longpass filter to a highly sensitive CCD camera. Videos were recorded using a customized longDaq software (Optical Imaging Ltd, Israel).*

A light emitting diode (LED) generated a blue light beam of 445nm wavelength with a constant 650 mA current. This blue light beam was redirected by the 495 nm dichroic longpass filter into the optical path of the camera. LED light passed through the chronic window on top of the skull into the cortex. Here, the blue light excited GCaMP6s protein to enhance its fluorescence. The emitted green light from the cortical GCaMP6s proteins passed back through the first reversed video lens (NIKKOR, 85 mm f1.4), the 495 nm dichroic longpass filter, the second lens (non-reversed, NIKKOR 50 mm f1.2) and a 515 nm longpass filter. The projected image was recorded by the CCD camera and using a customized longDaq software. Working distance between the mouse cortex and first video lens was approximately 4.4 cm (**Figure 4**). The camera field-of-view covered a quadratic area of approximately 12x12 mm = 144 mm^2 in the focused plane which allowed to acquire brain activity of the entire forebrain cortex. Data was spatially binned at 3x3 pixels, resulting in an image matrix of 330x330 pixels (**Figure 5**).

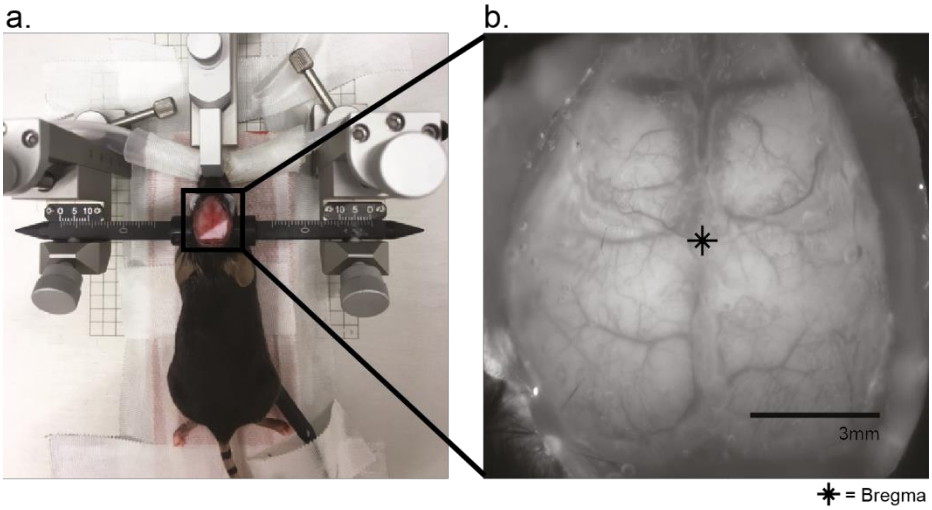

Figure 5: Top view of a mouse prepared for imaging and display of one image frame. a. *Image of a mouse with its head fixed in a stereotactic frame ready for imaging.* ***b.*** *Exemplary image frame of in vivo widefield calcium imaging is displayed. The entire forebrain cortex is included in image acquisition.*

2.2.2.2.3 Anaesthesia

As we decided to use anaesthetics in our imaging protocol, we aimed to characterize its effect on imaging parameters. Therefore, we evaluated three different anaesthesia protocols in our anaesthesia study: 1.5% ISO, 1.0% ISO and MED+ISO. Whereas the 1.5% ISO and the 1.0% ISO differed only in the dosage of isoflurane for anaesthesia maintenance (1.5% and 1.0% respectively), in the MED+ISO protocol we injected the animals 0.05mg/kg body weight of medetomidine intraperitoneally 5 minutes prior to inducing anaesthesia. Percentage of isoflurane for maintenance in the MED+ISO protocol was 0.75% only. All three anaesthesia protocols were then conducted in the same manner: Induction for 70 seconds with 5% isoflurane, 140 seconds of stabilization with 1.5% isoflurane, and final respective isoflurane dosage according to the protocol for at least 4 minutes before image acquisition to reach a stable anaesthesia state. In the final phase, input stimuli to the mice such as touch or noise were diminished to attain steady state. Isoflurane was vaporized in 30% O_2 and 70% N_2O. We performed resting state imaging for each mouse (n=9) at least three times per condition in a randomized order with at least one day of rest in between acquisitions.

To define functional networks (network study) and to assess changes in post-stroke functional connectivity (stroke study) only the MED+ISO protocol was used.

2.2.2.2.4 Resting state imaging

After anaesthesia induction, the animals head was fixed in a stereotactic frame. The stereotactic frame was used for two reasons: firstly, the jaw holder cuffs (product number: 51647 Stoelting, Europe) which were used to fix the head of the mouse at their jaws eliminated head motions. Secondly, regulating screws on the stereotactic frame allowed to adjust the skull plane horizontally (orthogonally to the optical path of the camera) for optimal recording conditions. Then, the chronic window was cleaned with ethanol and the eyes were shielded from light. The focal plane of the camera was set

about 1 mm below bregma. Mice were not touched at least 4 minutes before data acquisition. During acquisition the room was dark and quiet to create reproducible conditions for *resting state* with the lowest number of external stimuli possible to the mouse. Images were recorded at a frame rate of 25 Hz. To determine acquisition duration, we conducted a preliminary experiment with different acquisition times (**Figure 6**). To this end, we defined a recording time of 200 seconds (=5000 frames) for the anaesthesia study and 240 seconds (=6000 frames) for the remaining studies, as longer recording duration did not reveal any advantages.

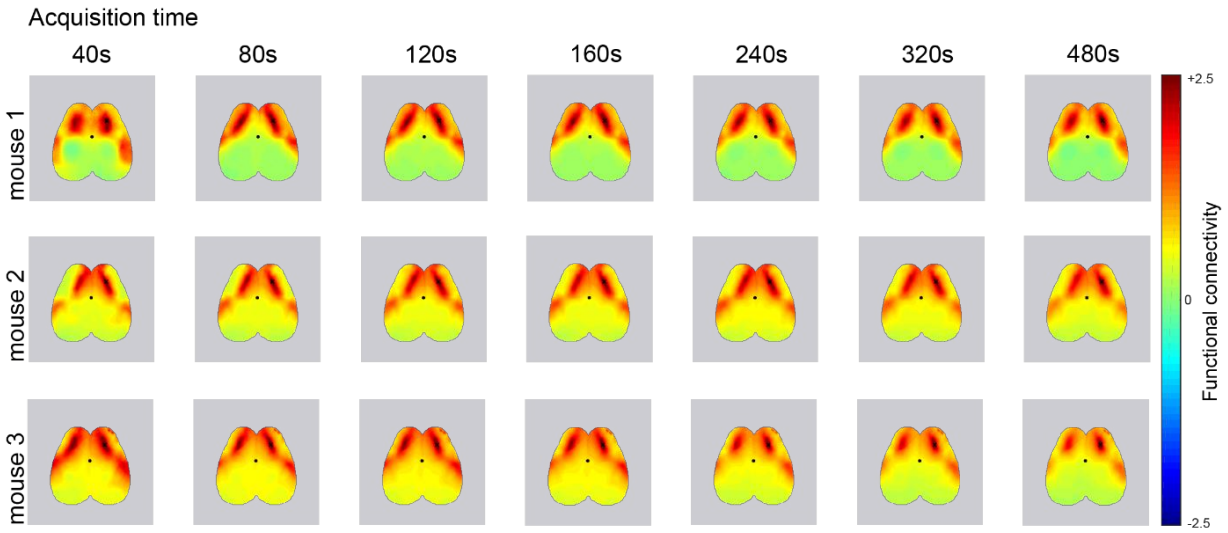

Figure 6: Exemplary comparison of effect of different acquisition durations on functional connectivity in three individual mice. *Functional connectivity analysis is displayed for each individual mouse for 40s, 80s, 120s, 160s, 240s, 320s and 480s recording time respectively. After 120 seconds no relevant changes in functional connectivity can be seen for longer acquisition durations.*

By using the PowerLab data acquisition system (PowerLab 16/35, ADInstruments, New Zealand) and LabChart (LabChart, ADInstruments, New Zealand) we were able to record vital parameters (heart rate and respiratory rate) simultaneously to *in vivo* widefield calcium imaging in some animals (n=6).

2.2.2.2.5 Stimulus dependent imaging

Following resting state imaging, stimulus dependent imaging was performed in a group of naïve animals (n=23). In order to conduct stimulation, acupuncture needles (Hwato, Ternimed, Germany) were inserted subcutaneously between the second and third digit of each paw. Stimulus was triggered by the Vdaq software (Optical Imaging Ltd, Israel), passed on to a Train/Delay Generator (DG2A, Digitimer Ltd, UK) and finally lead to a constant current isolated stimulator (DS3, Digitimer Ltd, UK) which stimulated the paw. The stimulation settings were specified in preliminary experiments combining two concepts: We wanted to acquire only sensory – not pain – response. But at the same time, stimulation had to be strong enough to reveal constant response in terms of effectively obtaining a cortical answer to the stimulus as often as possible. We realized this by reducing mainly the frequency and number of applied stimuli. Finally, we determined the subsequent protocol: We stimulated the paws alternating and for at least two imaging blocks. Each block consisted of 10 trials.

Every trial lasted 8 seconds and consisted of the periods: a two second baseline, a 4 seconds stimulation and a final 2 seconds resting period. Stimulation was conducted with maximum 1.6 mA amplitude, 300 ms duration and 1 Hz interval. We recorded stimulation dependent brain activity at 12.5 Hz frame rate.

2.2.2.3 Induction of stroke and assessment of lesion size

2.2.2.3.1 Photothrombosis

Photothrombosis is an established, experimental model to induce focal ischemia to a specific restricted cortical area. With help of photooxidation of the dye Rose Bengal (Sigma- Aldrich, USA) a thrombus is formed in illuminated blood vessels. In order to define the motor cortex to specify the target area, a resting state *in vivo* calcium imaging acquisition was obtained at least one day prior to stroke induction. A single-subject independent vector analysis (IVA, method described in 2.2.3.7) was calculated on the naïve data for each single individuum to reveal its motor cortex coordinates. Obtained coordinates were marked on the chronic window. 10 µl per gram body weight of 1% Rose Bengal dye in saline was injected in mice intraperitoneally (i.p.) 5 minutes prior to anaesthesia induction (5% isoflurane in 30%O2/70%N2O). The head of the anaesthetized animals was subsequently fixed in a stereotactic frame. The non-targeted area was covered to be shielded from laser light. We used a laser (Cobolt HS-03, Solna, Sweden) with a fibre optic bundle of 1.5 mm diameter at the tip, constant 561 nm wavelength and 25 mW output power at the fibre. To induce a lesion restricted to the area of interest the skull was illuminated for 17 minutes through the coverslip, the dental cement and the intact skull. Sham procedure was done correspondingly, but without laser illumination. After the procedure animals were allowed to recover in a heating chamber.

2.2.2.3.2 Laser speckle

Infarct area was quantified via laser speckle contrast imaging with a PeriCam PSI System (PeriCam PSI System, Perimed, Sweden), 24 hours after photothrombosis. For this procedure animals were lightly anesthetized to reduce motion artefacts. Blood flow was measured for 30 seconds and averaged. A color-coded depiction was created from the data measured by the laser speckle. Subsequently, the area of the cortex with strongly diminished perfusion was manually quantified using ImageJ software (Version 1.49c, Fiji)[45].

2.2.2.3.3 Quantification of autofluorescence in calcium imaging data

In addition, infarct area was quantified via autofluorescence in *in vivo* widefield calcium imaging data. As the necrotic brain tissue presented highly autofluorescent in our imaging data, we aimed to quantify this area. Saturated pixels within the masked area – and therefore within the cortical area – were identified. The identified pixels allowed to depict the infarcted area. For quantification number of saturated pixels was counted.

2.2.2.4 Behaviour testing

2.2.2.4.1 Beamwalk test

The beamwalk test was conducted by adjustments to a previously described protocol[46]. In this test, the mouse has to travers a narrow beam to reach a home cage. The animal is video recorded during this task, and its foot faults can be evaluated. To perform this test, we built a customized set-up: We used a 5x20 mm wooden testing beam and a 10x10mm training beam. The selected beam was laid on two bars at 50 cm height. On one end a home cage provided a save spot the mice were searching for. Mice had to travers 80 cm of the beam before reaching the home cage. A camera was placed on one side so the footsteps could be recorded. Mice underwent at least 3 days of training consisting of adaptation to the environment, balancing on larger beams (training beam) until they successfully crossed the testing beam without making breaks. A baseline run on the testing beam was recorded and after stroke data was acquired for day 3, 7, 14, 21, 28 and 56 after stroke. On each testing day, every mouse had to run three times with a 30 second break in the home cage in between. All trials were video recorded and analysed frame by frame. Foot faults of the hindlimbs were counted for each paw separately and averaged for all three runs per time point. We used 2-way-ANOVA and Dunnett's correction for multiple comparisons for statistical testing.

2.2.2.4.2 Neuroscore

The neuroscore was assessed as previously published[47]: Neuroscore is a composed score aiming to assess both global and focal deficits after stroke in mice. In total 0 to 54 points can be scored (26 point for general and 28 for focal deficits), a higher score representing worse deficits. Evaluation of global deficits included grooming, status of ears and eyes, posture, spontaneous activity and epileptic behaviour. Focal deficits were evaluated by assessment of gait, grip, forelimb-asymmetry during tail suspension, circling behaviour of both entire body or only forelimb, body symmetry and whisker response. Score was gathered once at baseline level and on day 1, 3, 7, 14, 21 and 28 after stroke. We used repeated measure 2-way-ANOVA and Sidak's correction for multiple comparisons for statistical testing.

2.2.2.5 Animal perfusion, tissue sectioning and GCaMP quantification

Before perfusion mice were intraperitoneally injected with ketamine (120 mg/kg) and xylazine (16 mg/kg). When animals were deeply anesthetized, they were transcardially perfused with PBS (20ml/animal) followed by 4 % PFA (20ml/animal). Brains were removed and immediately post-fixed in the same fixative overnight at 4 °C. Brains were cryoprotected by saturation in 30 % sucrose and stored at -80 °C until further processing.

2.2.3 Ex vivo experiments

2.2.3.1 Tissue sectioning and GCaMP quantification

Perfused and PFA-fixed brains were covered in optimum cutting temperature compound (O.C.T., Tissue-tek) solution and coronal sections of 20µm thickness cryo-sliced. Consequently, to enhance GCaMP fluorescence, sections were incubated in calcium saturated buffer ([0.9mM] calcium diluted in PBS) for 10 minutes. Slices were immediately analysed on a epifluorescence microscope (Zeiss, Germany). We used standard GFP filter and magnification of 5x, 10x, and 40x for GCaMP quantification (**Figure 3**).

2.2.4 Computational analysis of *in vivo* mesoscale calcium imaging data

2.2.4.1 Preprocessing

All data was processed in MATLAB (R2016b, The MathWorks, USA). During preprocessing we intended to diminish signal fluctuations caused by heart and respiratory rate as well as noise such as signal decay due to GFP bleaching by the light beam during acquisition. Preprocessing consisted of four steps:

- First, images were resized by the factor 2/3 to a 220x220 pixel matrix, using the MATLAB function imresize. This final matrix offered a resolution of 18.5 pixel/mm.
- Second, data was intensity normalized by calculating:

Equation 1

$$\frac{\triangle F}{F} = \frac{F_0 - F}{F}$$

where:

F equals to the mean fluorescence intensity of the signal time course as a reference

F_0 is the fluorescence values of a given time point

- Third, to reduce noise induced by vital parameters signal time course was filtered. A bandpass-filter from 0.1 to 1 Hz was created by using the MATLAB functions cheby1 and filtfilt to design a Chebyshev Type I filter of order 2 and to perform zero-phase digital filtering. Measured heart and respiratory rate were always between the upper cutoff frequency of our filter (1 Hz) and the Nyquist frequency of 12.5 Hz in a test data set, making their alias free removal by the bandpass filter (**Figure 7**). To account among others for the decay due to signal bleaching, the lower bound of the filter removed low frequency components.
- Forth, the signal time course was cropped 10 seconds from the beginning and the end before further analysis to eliminate possibly remaining filter artefacts.

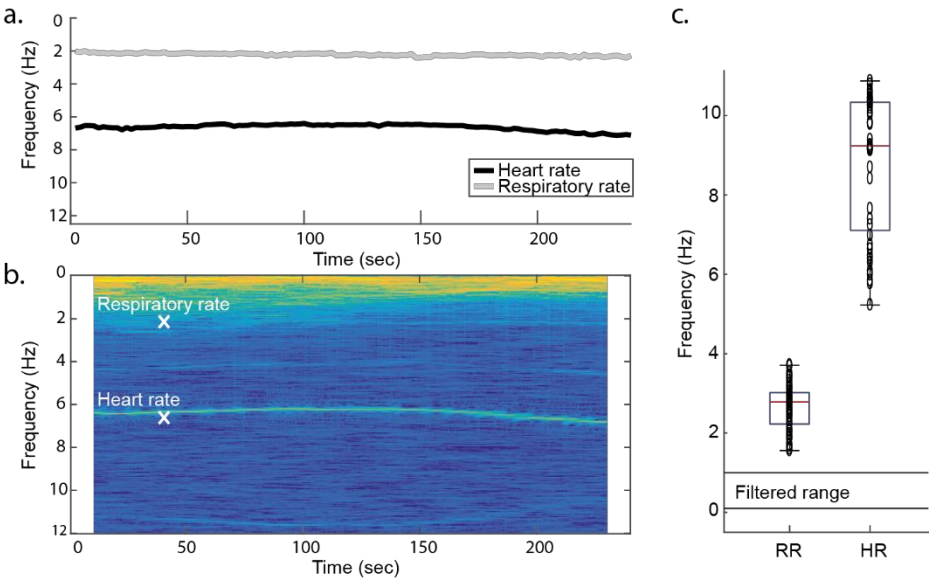

Figure 7: Potential interference of vital parameters in imaging data is eliminated by filtering. a. *Exemplary vital parameters (heart rate (HR), respiratory rate (RR)) simultaneously to data acquisition in one mouse.* ***b.*** *Spectrogram of unfiltered raw signal of the same acquisition as in a. Exemplary HR and RR are indicated by white crosses* ***c.*** *Mean HR and RR obtained per one resting state imaging in Hz; range of frequencies kept after filtering is indicated by black lines (n=6; >2recordings each)*

Performance of preprocessing is demonstrated in an exemplary raw signal and corresponding preprocessed signal time course in **Figure 8.**

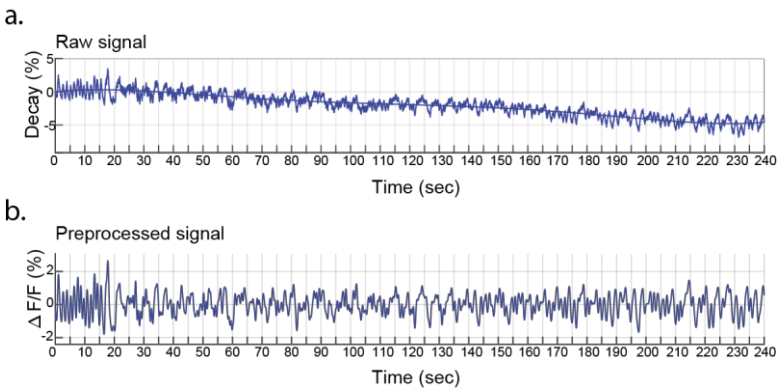

Figure 8: Exemplary signal time course before and after preprocessing. a. *The raw signal time course of one single pixel is depicted. Signal decay due to bleaching effects is prevalent.* ***b****. Signal time course after preprocessing. Signal is centred around its mean after calculation of ΔF/F.*

In preliminary experiments, we demonstrate GCaMP signal is the leading signal in our acquired data, this justifies that no further preprocessing was performed (e.g. to account for hemodynamic absorption) (**Figure 9**).

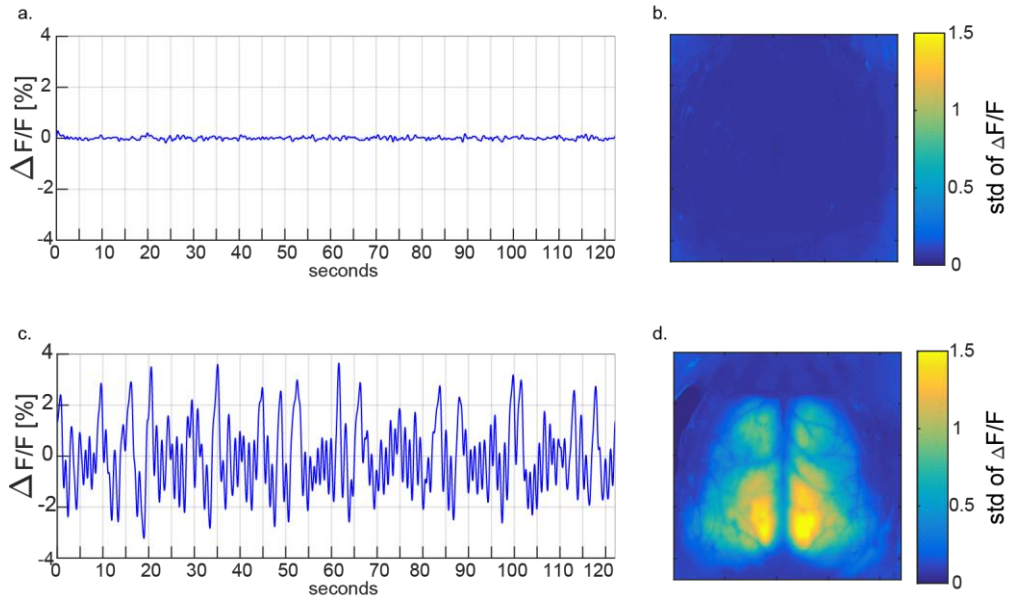

Figure 9: GCaMP fluorescence is dominating the acquired signal. a. *and* ***c.*** *Preprocessed signal time course of resting state imaging of a. a wild type littermate (Thy-1 GCaMP6s -/-) and c. a Thy1-GCaMP6s heterozygous mouse.* ***b.*** *and* ***d.*** *Standard deviation of each signal time course per pixel was calculated for the wildtype and Thy-1GCaMP6s heterozygous animal respectively. Calculated values are depicted topographically with a colour code.*

2.2.4.2 Data selection via movement analysis in videos of calcium signal

We generated videos of the preprocessed data for quality control of both data acquisition and preprocessing. Motion artefacts were of particular relevance for the data acquisition quality control. Therefore, I reviewed every single acquisition. As soon as one single movement was detected the recording was excluded from further analysis. Hereby, 3 acquisitions out of 30 were excluded for 1.5% ISO recordings (10% excluded), 11 acquisitions out of 41 for 1.0% ISO recordings were excluded (26,8% excluded) and 9 acquisitions out of 34 for MED+ISO protocol were excluded (26,5% excluded) for the anaesthesia study. In the stroke study, the final number of acquisitions was 256 (out of 279, 8.2% excluded).

2.2.4.3 Spatial registration

Data was repositioned with their bregma in the centre and the sagittal suture in the vertical line to compare recordings from both different mice and different time points. This spatial registration process was conducted by generating two transformation matrices: preprocessed images of the first acquisition of every individual mouse were manually rotated and translated in the image plane into a virtual space (3 degrees of freedom) and the information stored in a first matrix. The virtual space enabled the interindividual comparability. For the second matrix two steps were necessary. First, for all other acquisitions of the same individual were aligned to the first (non-repositioned) acquisition. Thereby, anatomical structures such as vasculature and sutures were visually overlapped. The resulting matrix was then combined with the first matrix, in order that every recording could be repositioned in the virtual space in one single interpolation step. This second step guarantees intraindividual correspondence (**Figure 10**).

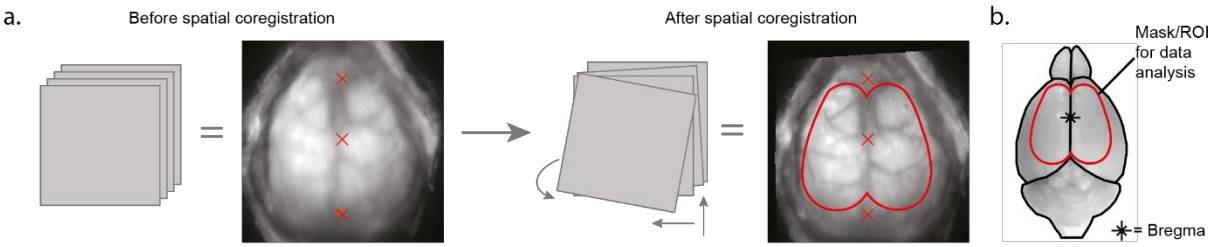

Figure 10: Scheme of the spatial registration and masking process. a. *Depiction of merged raw images of several recording of one individual mouse before and after spatial registration. The scheme left to the pictures show the registration process by rotating and translating. Red crosses display the reference marks in the virtual space frontal suture, bregma and sagittal suture (from top to bottom). After spatial registration the overlapped images appear less blurry as for example vessels can be better distinguished than before registration. Red line indicates the masked area.* ***b.*** *Schematic comparison of the size of mask and mouse brain*

2.2.4.4 Masking of the images

We generated a mask for each individual acquisition to feed only those areas of the complete image into the analysis which are anatomically relevant and of good acquisition quality. This mask was created by combining a "general" and "individual mask". The "general mask" was obtained by manually comparing the registered images from different animals and choosing an analysis area which symmetrically covered both brain hemispheres. The purpose of this mask was to include only cortical areas within the focal plane and exclude more lateral parts which were due to the curvature of the skull out of focus (**Figure 10b,** red line). The "individual mask" was generated computationally and masked all saturated pixels. Those saturated pixels originated from autofluorescence e.g. in areas impaired by stroke. Its function was to eliminate pixels without signal fluctuation and therefore potential artefactual impact on the analysis. The combination of the two masks was used for all further analysis and allowed the identification of all included signal time courses.

2.2.4.5 Power spectrum calculation and frequency-based parameters

Power spectral densities (or simply power spectra) were computed by the MATLAB function periodogram. Spectrograms were computed by calculating the power spectral density within a moving window of 250 frames (=10sec), moving frame-by-frame over the entire signal time series. An exemplary spectrogram and heart and respiratory rate for the same acquisition are depicted in **Figure 7**. There, power spectra were computed for 6 arbitrarily preselected pixels and subsequently averaged. In the anaesthesia study, the power spectrum was computed after preprocessing of three arbitrarily selected pixels in the right hemisphere and averaged. Spectral edge frequencies (SEF) and median frequency (MF) were calculated as the frequencies where the cumulative power reached respectively 5% (SEF 5), 50% (MF) and 95% (SEF 95) of the total power. A paired t test with subsequent Bonferroni correction was used for statistical testing of group differences in the anaesthesia study.

2.2.4.6 Data selection via ApEn

We assessed depth of anaesthesia to ensure reproducible and stable experimental conditions. With help of this assessment comparability of the recordings of brain activity throughout experiments should be generated. We used approximate entropy (ApEn) to estimate the degree of randomness and system complexity[48]. We used the algorithm described in detail by Pincus et al.[48]. ApEn was computed for preprocessed data for three arbitrarily chosen pixels within the right hemisphere. We used the MATLAB file exchange function to compute fast approximate entropy, as described by Kijoon Lee[49]. We used the commonly used embedding dimension m=2[50]. ApEn was then computed for a range of tolerance levels (tolerance=r*std, with the coefficient r being varied between 0.01 to 0.3 by steps of 0.01, and std being the standard deviation of the signal time series). Then ApEn levels were averaged across the three pixels for each tolerance level separately and the maximum was evaluated. This maximum approximate entropy ($ApEn_{max}$) was chosen to reflect the appropriate value best as discussed by Chon et al [50]. Paired t test and following Bonferroni correction served for statistical testing of group differences in the different anaesthesia protocols.

To identify an appropriate anaesthesia protocol with only moderate impact of anaesthesia on imaging data, ApEn was determined. Paired t test and following Bonferroni correction served for statistical testing of group differences in the different anaesthesia protocols.

Evaluations between the different anaesthesia protocols reveal a necessary threshold of $ApEn_{max}$ equal to 1.25. All recordings having a lower value, which was associated with deeper anaesthesia, were excluded from the stroke study (4 out of 279 acquisitions =1.4% of the recordings).

2.2.4.7 Independent vector analysis

In order to determine functionally independent cortical networks an independent vector analysis (IVA) was performed. Therefore, we implemented the Group ICA of fMRI Toolbox (GIFT v3.0a; http://mialab.mrn.org/software/gift) in our protocol. The IVA is an extension of independent component analysis (ICA). It allows analyse grouped data[51–53] and is an alternative to the often applied group independent component analysis (GICA). IVA could be shown to better maintain the variability of the single subjects[54]. Hence, IVA allowed us to compute both cross-sectional and individual single subject analysis. Cross-sectional analysis of a set of naïve animals provided regions of interest (ROI) for further analysis, while the single subject analysis revealed coordinates of the motor cortex before stroke induction for each individual animal. To identify the latter, we chose the component whose spatial map was located rostrolateral to the bregma –the motor cortex of the forepaw— and its peak pixel served as coordinates for stroke induction. The peak pixel is defined as the pixel with the highest correlation of its signal time course to the signal time course of the component.

The algorithm to perform an IVA needed a preselected number of components to be found. For single subject analysis 20 components were estimated and the cross-sectional group analysis was performed with increasing numbers of components (i.e. 16, 18, 20 and 30). IVA was performed on preprocessed

data for naïve animals only. Only signal time courses within the masked brain were feed in to identify independent components.

2.2.4.8 Definition of functional networks and ROI

We aimed to define functional cortical areas across all animals to use those areas for functional connectivity analysis. A meta-analysis of several group IVA was performed to accomplish very robust results. 16 group IVAs were computed with the following conditions: Two different large groups of naïve animals (n=41 and n=47), each animal was recorded on two independent days with at least one day in between for 4 minutes (=6000 frames). This resulted in 4 different data sets which were consequently analysed. We then performed four IVAs by requesting 16, 18, 20 and 30 components. Out of the resulting 16 group IVAs, 10 were chosen in which the spatial maps were topographically congruent and represented in multiple analyses. Finally, only components were selected which were revealed in at least 9 out of 10 analyses, less represented components were not considered as robust and discarded. The spatial maps of the components were merged and the median of their peak pixel calculated. Circular areas of 49 pixel (= 8 pixel diameter ≈0.43 mm) around those median peak pixel were defined as regions of interest (ROI). We chose ROIs in the sensorimotor system – four on each hemisphere – to analyse functional connectivity. To this end all signal time courses within the ROI were extracted, their mean determined, and the mean signal time course was utilized for functional connectivity calculation. The aim of averaging the signal was to reduce possible noise in single pixel time courses. However, the masking step described above also served as a criterion to include single ROIs into analyses. If a ROI was located within or at the edge of a cortical area affected by autofluorescence, this ROI was excluded from the analysis. More specifically, only if more than 75% of the pixel within a single ROI were situated within the mask, the ROI entered analysis. Here, only signal time courses within the mask were averaged to obtain the mean signal time course of the ROI.

2.2.4.9 Functional connectivity

We used functional connectivity to investigate changes in brain network architecture in both the anaesthesia and the stroke study. In the former we wanted to determine the impact of anaesthesia on functional networks whereas in the latter the effect of stroke on brain activity and the process of its recovery was observed. For this purpose, we used four different analysis strategies: ROI pair-wise functional connectivity, seed-based functional connectivity, quantification of contralateral motor size and global connectivity. The last two were only used in the stroke study.

Functional connectivity was defined as the Pearson's correlation between two time series with the following equation (**Equation 2**).

Equation 2

$$CM = \frac{\sum_{i=1}^{n}(X_i - \bar{X})(Y_i - \bar{X})}{\sqrt{\sum_{i=1}^{n}(X_i - \bar{X})^2}\ \sqrt{\sum_{i=1}^{n}(Y_i - \bar{Y})^2}}$$

where:

n is length of the time series

X_i, Y_i are the individual sample timeseries indexed with i

$\bar{X} = \frac{1}{n}\sum_{i=1}^{n} X_i$ = the sample mean; and analogously for $\bar{Y}$

Values of the correlation coefficient *CM* can vary between –1 and +1. A value of –1 implies perfect negative correlation (or anticorrelation), whereas a value of +1 implies perfect positive correlation. A Pearson's correlation value of 0 indicates no correlation between the signal time courses. Pearson's correlation coefficients were calculated in between signal time series of different ROI (as resulting from the IVA meta-analysis) and between ROI and single pixel time series. Consequently, the obtained Pearson's correlation coefficients were Fisher z-transformed (**Equation 3**), to enable parametric statistical testing and to gain more detailed assessment of high connectivity levels.

Equation 3

$$CMz = 0.5 * \log\left(\frac{1 + CM}{1 - CM}\right)$$

The resulting Fisher z-transformed correlation values can range from -2.5 and +2.5, with – analogous—values of -2.5 indicating perfect negative correlation and a value of +2.5 indication perfect positive correlation. A value of 0 indicates no correlation of the signal time courses. The Fisher z- transformed Pearson correlation values between two signal time series are called functional connectivity values in the following.

2.2.4.9.1 ROI pair wise functional connectivity

In this analysis, functional connectivity was computed between ROIs. We selected in total 8 ROIs of the sensorimotor cortex in both hemispheres: rostral forelimb (RFL) and caudal forelimb motor cortex (CFL), forelimb (FLs) and hindlimb sensory cortex (HLs). Correlation was computed between each possible combination of ROIs resulting in 28 functional connectivity values. The results were depicted as graphs and matrices. In the graph depiction, the functional connectivity between two ROIs was represented topographically by a color-coded line connecting the centres of corresponding ROIs, an exemplary mouse cortex in the background. The same colour code displayed the connectivity values in the matrix.

2.2.4.9.2 Seed-based functional connectivity

Seed-based functional connectivity was defined as the correlation between a selected ROI in the right caudal forelimb (rCFL; here considered the seed of analysis) and the signal time courses of all pixels within the masked cortex, respectively. All connectivity values were depicted as a color-coded topographical map.

2.2.3.9.3 Averaging and statistical comparison of functional connectivity values

In the anaesthesia study, three recordings per condition per animal were acquired. First, connectivity values were averaged across trials within condition, but for each mouse separately. Then, paired t tests and Bonferroni correction were used to assess differences in the average scores between conditions. Finally, scores were averaged across mice within each anaesthesia condition for visualization.

In the stroke study, one acquisition per animal per timepoint was obtained. First, the connectivity value for of a specific ROI-pair or ROI-pixel-pair was excluded from analysis entirely, if the masking process let the sample size drop below 5 animals per group (i.e. stroke or sham group). Then, two sample t test and Bonferroni correction were used for statistical comparison between stroke and sham groups at each time point. Here, connectivity scores were averaged across mice within the single time points for graphical depiction.

2.2.4.9.4 Quantification of contralateral motor cortex size

The contralesional motor cortex area was quantified after calculation of seed-based functional connectivity in the rCFL. Assessment of the size of the rCFL was done by summing up pixels with functional connectivity values > 2.25 in the same hemisphere only. The resulting values were normalized to baseline by dividing through the baseline value for each animal separately. This resulted in the fold change of the size of the motor cortex. Two sample t test and Bonferroni's correction was used for statistical analysis to reveal difference in sham and stroke group.

2.2.4.9.5 Global connectivity

Global connectivity analysis[55,56] was used to study more general changes in functional connectivity after stroke. More specifically, we were interested in alterations in the unaffected, contralateral hemisphere. Hence, global connectivity was calculated for each pixel within this area. To this end, the average of all functional connectivity values between one pixel and all other pixels in this hemisphere was calculated. This procedure was repeated for each pixel within the mask, resulting in one single connectivity value per pixel in the contralateral hemisphere. To analyse absolute changes in global connectivity after stroke, baseline levels were subtracted for each time point after stroke or sham procedure for every mouse separately. For statistical analysis the mean global connectivity of the contralateral hemisphere was obtained for each individual mouse, resulting in one single value per animal. Two-sided t tests with Bonferroni correction was utilized to assess group differences between treatments. For visualization though, the absolute changes in global connectivity were averaged within group and topographical color-coded map was generated for each time point and group.

In addition, global connectivity alterations were analysed creating a histogram of the distribution of non-normalized global connectivity scores across pixels. We performed this analysis for Baseline, D1 and D28 after stroke. Therefore, global connectivity scores were averaged across mice per time point and pixel, for the stroke and the sham group respectively.

2.2.4.10 Stimulation evoked activity

First, normalization of the recorded signal time series during paw stimulation was conducted by calculating:

Equation 4

$$\frac{\triangle F}{F_b} = \frac{F_0 - F_b}{F_b}$$

where:

F_b equals to the mean fluorescence intensity of activity recorded during the first two seconds as a baseline reference and F_0 is the fluorescence value of a given time point

Subsequently, processed data was averaged across trials within every individual mouse and the stimulated paw. We measured a stimulation-to-peak response delay of approximately 380ms in preliminary experiments. We defined frames recorded within a time window of 300-460ms after stimulus onset as peak of response and frames recorded within a time window 780-940ms after stimulus onset as trough of response. After extracting the peaks and troughs of response, frames were averaged within condition and peak to trough amplitude calculated as the difference between these averages. The intraindividual peak to trough amplitudes for stimulations at different experimental days were averaged for all four paws per mouse. In order to receive an average response across all mice the mean per condition was calculated. Subsequently, all pixels with a mean peak to trough amplitude above the 98th percentile were defined as the somatosensory core region. This region was considered to represent the stimulated paw area in the somatosensory cortex.

2.2.4.11 Statistical analysis

Statistics for behaviour testing have been calculated in Graph Pad Prism. Statistics for *in vivo* calcium imaging experiments have been performed in MATLAB. The statistical test is specified in the respective methods section.

3 Results

The overall aim of this study was to establish a translational imaging modality in mice. We chose to use the GECI-based imaging modality *in vivo* widefield calcium imaging. We enhanced the procedure to a translational level by transferring analysis paradigms commonly used in fMRI connectivity studies in humans to our transgenic approach in Thy1-GCaMP6s heterozygous mice. To achieve this, we performed a stepwise study design in three sub-studies, first analysing a stringent mouse sedation protocol, then identifying independent functional cortical areas via IVA and finally establishing network analyses in an experimental stroke model.

The anaesthesia study aimed to establish a sedation protocol allowing for stable and reproducible recordings of resting state neuronal activity and to derive physiologically meaningful functional connectivity scores. This study revealed a tremendous impact of anaesthesia depth on various imaging parameters which we consequently accounted for. The network study aimed to define functional cortical networks and to identify nodes in these networks which can be used as ROIs for functional connectivity analysis in mice. We were able to detect functionally distinct cortical areas in resting state data and to assign physiological brain function to them. The stroke study aimed to assess functional connectivity alterations after experimental stroke using the paradigm developed in the anaesthesia and network studies. We investigated both acute and chronic changes in functional connectivity after motor cortex lesion. While the acute phase was dominated by entire network disruption, diminished interhemispheric functional connectivity in functionally associated brain areas prevailed in the chronic phase.

3.1 Anaesthesia

In order to achieve our first aim to determine the most appropriate anaesthesia protocol for this imaging modality, we tested three different protocols and their impact on various parameters gathered during *in vivo* widefield calcium imaging analysis. We conducted this experiment in 9 animals and each mouse at least three times per condition with sufficient resting period in between. Resting state imaging was acquired using one of the following conditions:

1. Deep anaesthesia with 1.5% isoflurane inhalation (= **1.5% ISO**)
2. Low anaesthesia at 1.0% isoflurane inhalation (= **1.0% ISO**)
3. Light sedation with a combination of 0.05mg/kg bodyweight medetomidine injection and 0.75% isoflurane inhalation (=**MED+ISO**)

During analysis we investigated both frequency-based parameters and functional connectivity scores.

3.1.1 Impact on frequency-based parameters

First, we examined the preprocessed GCaMP signal of the three anaesthesia protocols. The effect on the signal time course of brain activity during the different protocols was directly visually evident (**Figure 11**). With decreasing depth of anaesthesia maximum amplitude of the signal time course appeared to be lower whereas the frequency dominating the signal seemed to be higher.

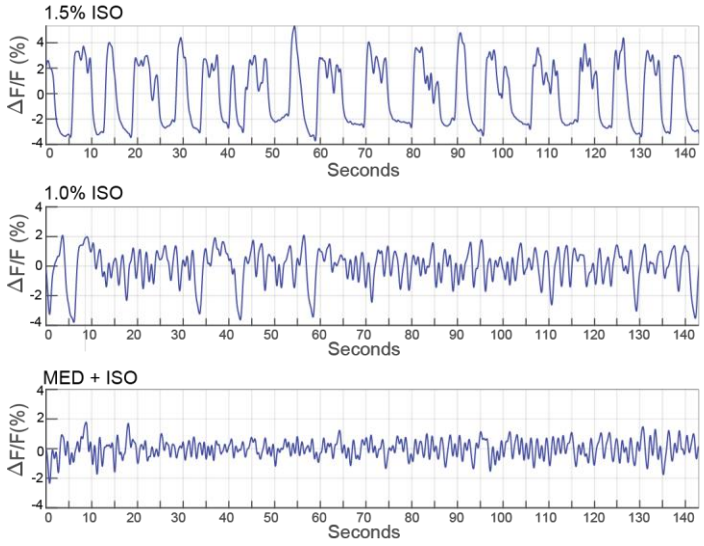

Figure 11: Anaesthesia influences signal time course of in vivo calcium imaging. *The signal time course of all three different anaesthesia protocols is depicted. For each condition 140 seconds preprocessed raw signal is displayed. All three examples show the same individual mouse.*

To quantify this impression, we computed different frequency-based parameters. We calculated power spectra for the signal time course and their derived spectral edge frequencies (SEF, 5th and 95th percentile) and median frequency (MF, 50th percentile).

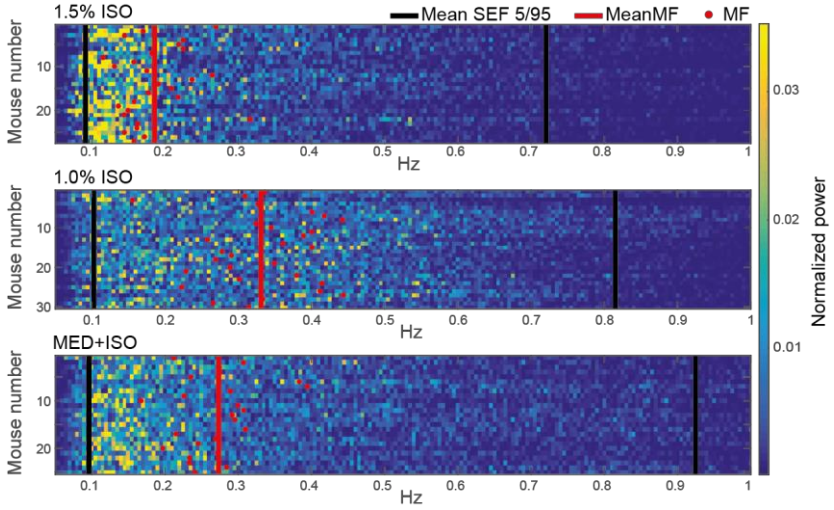

Figure 12: Power spectra and frequency-based parameters of all three anaesthesia conditions. *Power spectra are normalized to total power, analysis of each recording is displayed individually. Black lines indicate mean SEF 5 and SEF 95 (from left to right), red line indicates mean MF while red dots indicate the MF of each individual mouse.*

The power spectrum depicts the prevalence of each frequency within the filtered range (0.1-1 Hz) in the signal time course. The derived parameters MF, SEF5, SEF95 reflect the frequency at 50th, 5th and 95th percentile of cumulative power. The power spectrum revealed high power in low frequencies (0.1-0.2 Hz) in the 1.5% ISO group, whereas the other two anaesthesia groups showed much broader power spectra. This is underlined by a wider range of SEF5 to SEF95 in the 1.0% ISO and MED+ISO groups (**Figure 12**).

Correspondingly, analysis of all three anaesthesia protocols revealed significant differences in SEF95 between the three anaesthesia protocols (**Figure 13**).

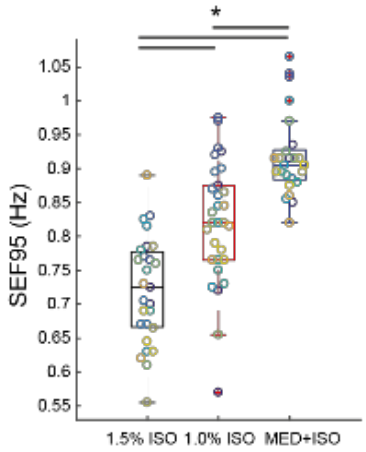

Figure 13: Spectral edge frequency at 95th percentile (SEF 95) of all three anaesthesia groups. *Each colour indicates a different mouse, each mouse was recorded at least three times per condition in a randomized manner. Significance bars above the plot indicate differences between conditions at a significance level α= 0.05.*

3.1.2 Impact on functional connectivity

In future experimental set-ups, we aimed to investigate functional connectivity in both brain disease and treatment experiments. To obtain meaningful results, we needed to examine the impact of anaesthesia on this analysis, to control possible confounding factors. We calculated both seed-based and ROI pair-wise functional connectivity within the sensorimotor cortex (**Figure 14**).

The effect of anaesthesia on seed-based functional connectivity analysis was already apparent on visual inspection. The 1.5% ISO group presented with higher functional connectivity scores than the other two protocols. The more detailed ROI-pairwise underlines this finding. Here, functional connectivity between each ROI-pair was calculated and displayed as a matrix. Closely all functional connectivity values of these ROI-ROI connections differed significantly between the deeper anaesthesia (1.5% ISO) group and both lighter anaesthesia groups (1.0% ISO and MED+ISO). In comparison, no difference was detected between the two lighter anaesthesia groups, the 1.0% ISO and the MED+ISO group. This analysis revealed a considerable effect of anaesthesia on functional connectivity which underlines the need to control the depth of anaesthesia in our experimental set-up.

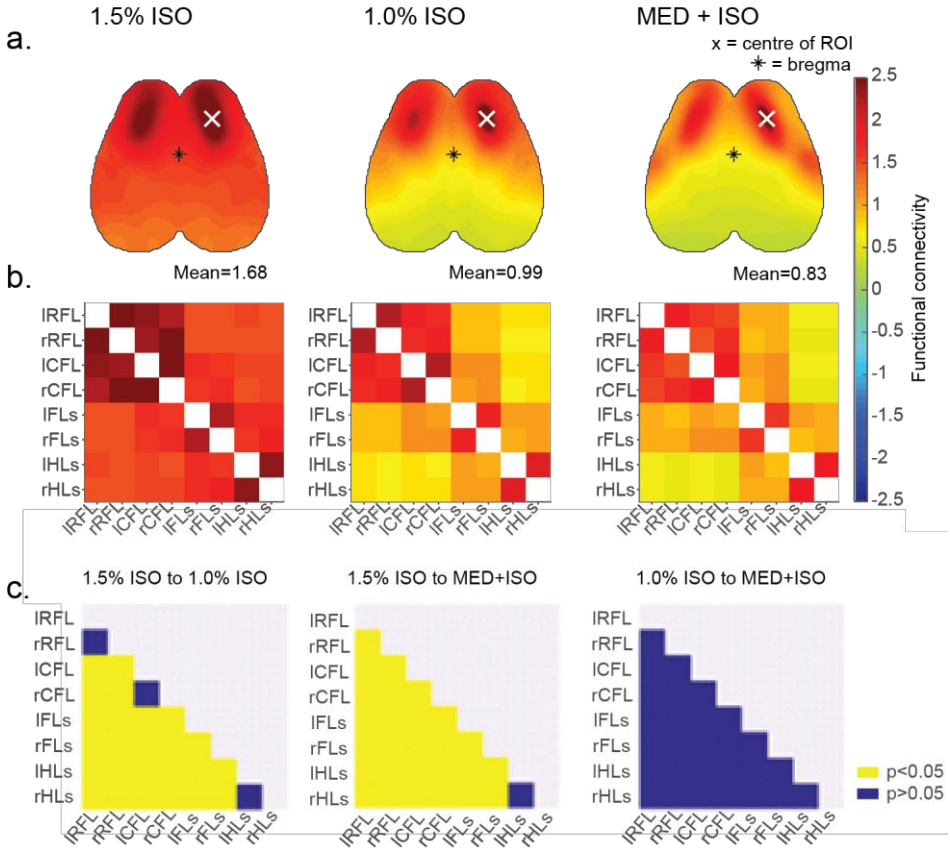

Figure 14: Influence of anaesthesia on functional connectivity. ***a.*** *and* ***b.*** *Functional connectivity values are averaged first across each individual animal per condition then across animals within condition.* ***a.*** *Topographical depiction of seed-based functional connectivity analysis. The seed placed in the right hemisphere is indicated by a white cross.* ***b.*** *Matrix of ROI pair-wise functional connectivity.* ***b.*** *and* ***c.*** *ROIs are placed in rostral forelimb (RFL), caudal forelimb (CFL), hindlimb sensory (HLs) and forelimb sensory (FLs) while r and l indicate right or left hemisphere. Seed definition is explained in detail in 2.2.3.8, 3.2.1 and Figure 16.* ***c.*** *Results of t test for statistical testing between groups. Yellow squares indicate significance with p-corrected<0.05 in corresponding connections.*

3.1.3 ApEnmax to distinguish anaesthesia conditions

In a third analysis, we aimed to identify a parameter which is capable to distinguish our three experimental protocols. This parameter further could serve to monitor depth of anaesthesia in subsequent experiments. We calculated maximum approximate entropy—a measure of randomness and system complexity. This parameter differed significantly between all three anaesthesia groups (**Figure 15**). The highest entropy values were detected in the sedation protocol (MED+ISO). Additionally, the deep anaesthesia (1.5% ISO) and sedation (MED+ISO) protocol did not reveal any intersection values of $ApEn_{max}$ which makes this parameter sensitive to distinguish between these two protocols. The MED+ISO protocol offered the widest spread in the frequency spectrum and was subjectively the most reliable to handle protocol. Due to these considerations, we decided to use this protocol for the subsequent sub-studies: the “network study” and the “stroke study”. In order to control

the possible impact of deeper anesthetized animals, we defined a cut off $ApEn_{max}$ value of ≤1.25 to exclude affected recordings.

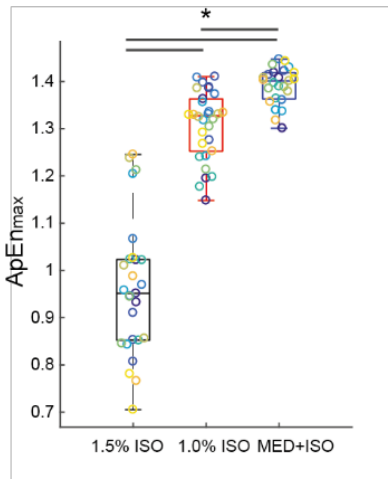

Figure 15: $ApEn_{max}$ levels of all three anaesthesia groups. *Each colour indicates a different mouse, each mouse was recorded at least three times per condition in a randomized manner. Significance bars above the plot indicate differences between conditions at a significance level α= 0.05.*

3.2 Network

For functional connectivity analysis it is necessary to determine preselected ROIs. In order to define those, we aimed to identify functionally relevant cortical networks in the mouse brain *in vivo*. We first identified independent cortical areas via IVA and then validated the result with both an anatomical atlas and stimulus-evoked brain activity. The resulting functional cortical areas were subsequently defined as ROIs.

3.2.1 Network definition via resting state imaging

Independent vector analysis (IVA) can be applied on resting state imaging data. This analysis can identify independent cortical networks. To increase stability and reliability of the identified networks, we performed a meta-analysis of 10 group-IVA which were obtained from different data sets and parameters (for more details see method section). This meta-analysis yielded 12 components with similar spatial patterns in at least 9 out of the 10 IVAs (**Figure 16a**). In order to merge the analyses and retrieve a single area for each of these 12 components, the corresponding spatial maps were overlaid and the area where at least four analyses were above a predefined threshold per component was interpreted as belonging to one cortical network (**Figure 16b,** orange pixel). Additionally, each of these 12 components had a peak pixel in each hemisphere. The peak pixel is defined as the pixel with the highest correlation of its signal time course to the signal time course of the respective component. We calculated the median peak pixel coordinates across all IVAs within one spatially overlapping component for each hemisphere. The individual peak pixel of all IVAs were on average only 3.2 pixels (≈0.17 mm) distant from the resulted median peak pixel (**Figure 17i**). The median peak pixel

defined subsequently the coordinates of the midpoint of the respective ROI as being considered as the functional centre of cortical areas within brain networks such as the sensorimotor area (**Figure 16b**).

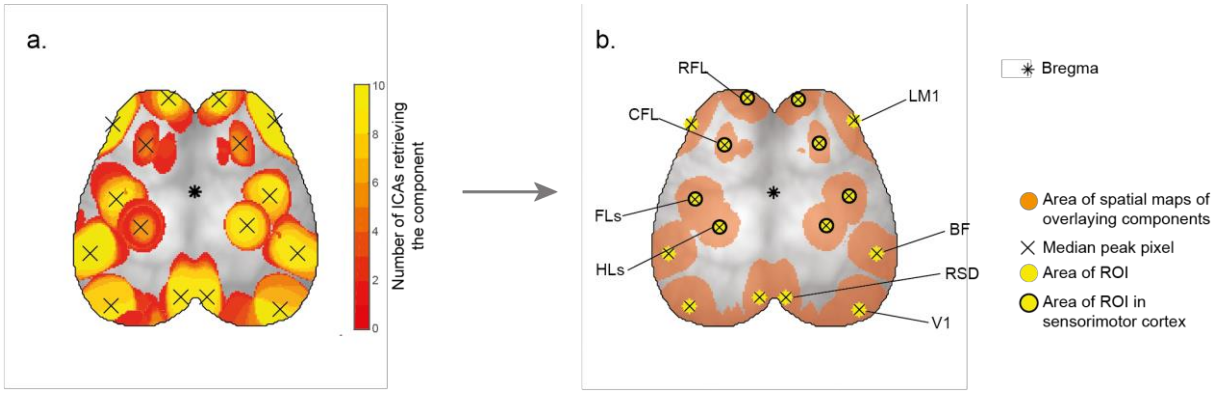

Figure 16: Identification of functional networks via IVA. a. *Result of a meta-analysis of 10 selected group IVAs depicted as a topographical heatmap with 12 retrieved components. Colour code mirrors how many of the group-IVA contained a certain pixel* ***b.*** *Definition of ROI which were used in further analysis (yellow). Centre of the ROI (crosses) is defined as the median peak pixel of a matching component retrieved in the meta-analysis. ROIs were anatomically labelled: rostral forelimb area (RFL), lateral M1 motor cortex (LM1), caudal forelimb area (CFL), forelimb sensory (FLs), hindlimb sensory (HLs), barrel field (BF), retrosplenium (RSD) and primary visual cortex (V1). ROIs within the sensorimotor cortex which were subsequently used to investigate functional connectivity changes in the stroke study are highlighted with a black circle.*

3.2.2 Network confirmation via Atlas based coordinates of functional cortical areas

In a second step, we aimed to validate morphological correlates of the 12 selected components by referring them to anatomically defined brain regions. This evaluation was conducted by collating the coordinates of the median peak pixel of each identified component to the Paxinos Brain Atlas[57] (**Table 1 and Figure 17)**. Each one of the 12 components could be clearly allocated to a functionally defined anatomical cortical area.

Table 1: Distance from median of peak coordinates of selected components to Bregma

COMPONENT NAME	rostral (-) / caudal (+) [mm]	left (-) / right (+) [mm]
left rostral forelimb (lRFL)	-2.91	-0.81
right rostral forelimb rRFL	-2.86	+0.76
left lateral M1 motor cortex (lLM1)	-2.10	-2.54
right lateral M1 motor cortex (rLM1)	-2.21	+2.48
left caudal forelimb (lCFL)	-1.46	-1.51
right caudal forelimb (rCFL)	-1.51	+1.40
left forelimb sensory (lFLs)	+ 0.22	-2.43
right forelimb sensory (rFLs)	+ 0.11	+2.32
left hindlimb sensory (lHLS)	+1.08	-1.67
right hindlimb sensory (rHLs)	+1.02	+1.62
left barrel fielf (lBF)	+1.89	-3.24

right barrel field (rBF)	+1.89	+3.18
left retrosplenium (lRSD)	+3.24	-0.43
right retrosplenium (rRSD)	+3,24	+0,38
left primary visual cortex (lV1)	+3,51	-2,59
right primary visual cortex (rV1)	+3,61	+2,64

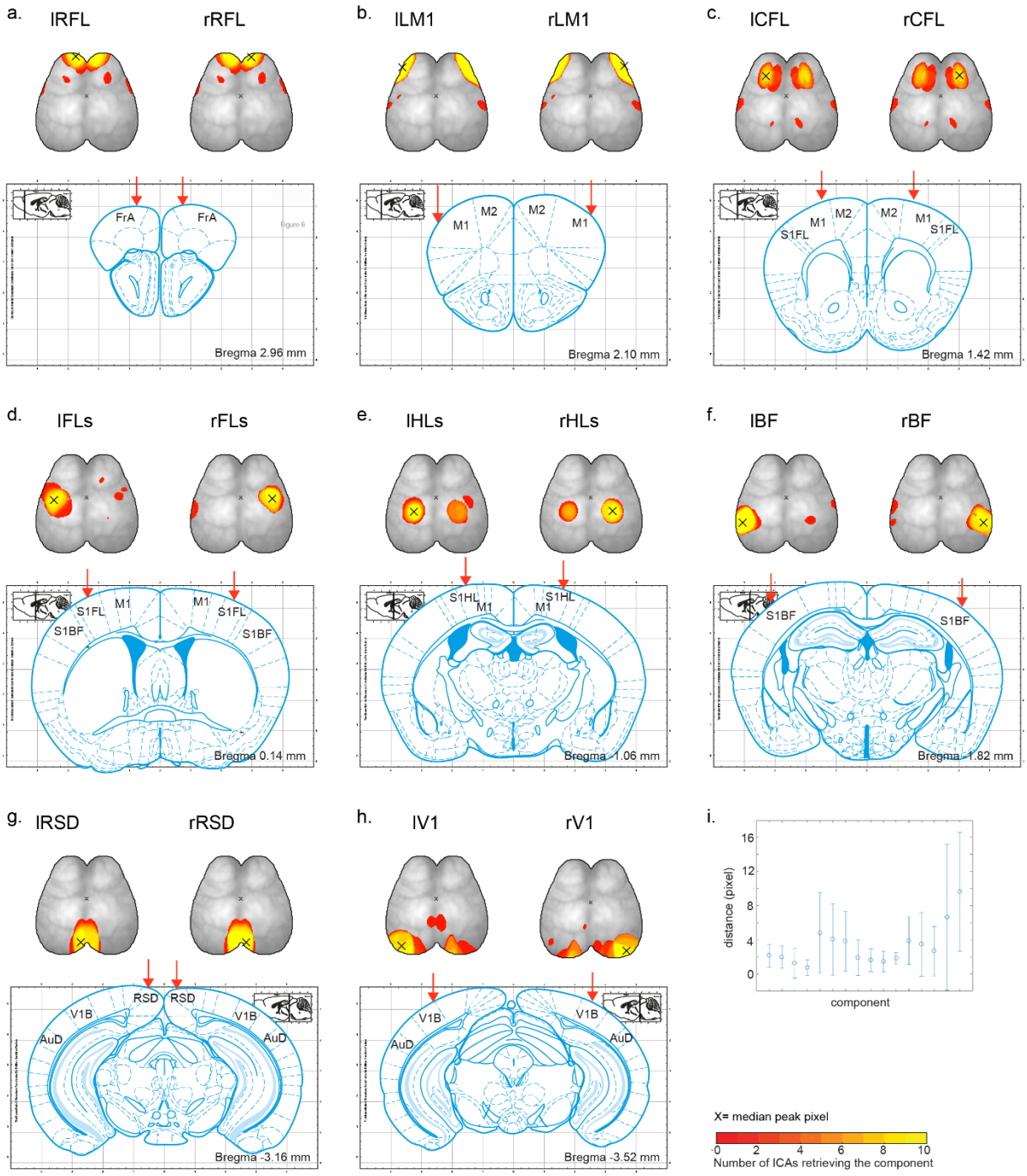

Figure 17: Coordinates retrieved by independent vector analysis (IVA) match anatomically defined functional cortical areas. *At the top, panels* ***a-h*** *depict the spatial maps of independent components selected from the reference IVA meta-analysis. If different but very similar components (i.e. matching when mirrored across the midsagittal line) presented*

*homotypic areas in the left and right hemisphere, they were displayed in the same panel, on the left and right side respectively. This applies to panel **d, e, f** and **h**. Peak pixel are indicated by black crosses. Below, coronal slides from the mouse brain atlas by Franklin and Paxinos[57] are shown. Slides were selected according to the anterior-posterior position of the peak pixels of each component. Referring these peak pixel coordinates to the atlas enables to label each component map. We assigned components with the peak in the respective area corresponding to the rostral forelimb area (RFL, **a.**), lateral M1 motor cortex (LM1) (**b.**), caudal forelimb area (CFL, **c.**), forelimb sensory (FLs, **d.**), hindlimb sensory (HLs, **e.**), barrel field (BF, **f.**), retrosplenium (RSD, **g.**) and primary visual cortex (V1, **h.**). Homotypic areas in the left and right hemisphere were mostly presented in distinct component maps with very similar (i.e. symmetric) component maps. Therefore, two component maps are displayed (two different ones in panel **d, e, f, h**), with l indicating left hemisphere and r indicating right hemisphere. The medio-lateral location of the component peaks is demonstrated by arrows in the slides of the atlas. **i.** Error of each median peak pixel calculated as the distance between the peaks of the individual component maps and the median coordinates of these peaks. Subsequently, the median coordinates defined ROI centre coordinates.*

3.2.3 Network confirmation via stimulation dependent imaging

In a last step we aimed to test the *in vivo* functionality of the cortical area defined by the selected independent components. Here we made use of a stimulus dependent imaging paradigm. We chose a sensory stimulus to induce a brain response in cortical areas which are involved in sensory processing. We electrically stimulated all 4 paws (n=23; **Figure 18**) while recording brain activity. Indeed, we observed a specific response to the sensory cortices of each paw which were again identified with the help of the Paxinos atlas[57] (**Figure 18b**). As expected, there was no response of non-involved cortices such as the motor cortex to the stimulus.

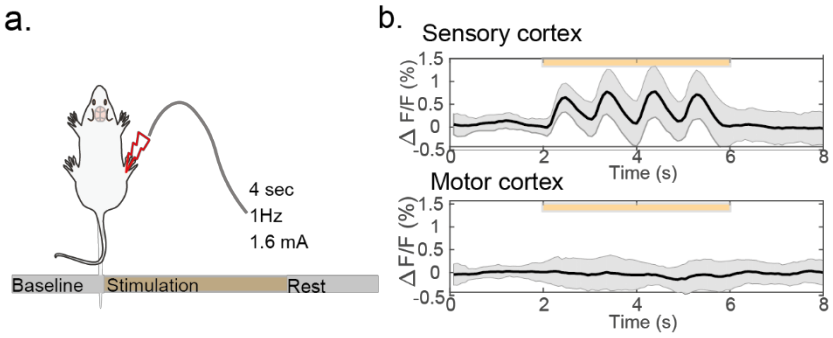

***Figure 18: Stimulus evoked brain activity is specific to sensory cortex. a.** Scheme of the experimental design for the stimulation dependent imaging. Total protocol of 8 seconds was divided in 2 seconds baseline recording, 4 second stimulation and 2 seconds resting period. Stimulation consisted of 4 1 Hz stimuli of 1.6 mA amplitude and 300ms duration. **b.** Exemplary hind limb stimulation of one animal. Signal time courses of contralateral sensory and motor cortex were averaged. The evoked response (mean (black line) and range of standard deviation (grey area) is displayed over time. Stimulus activated specifically sensory cortex.*

Right and left stimulation resulted in symmetrical activated brain regions. More specifically, the activated brain region was restricted to the contralateral sensory cortex whereas other cortical networks such as the motor system did not respond to the stimulus (**Figure 19a**). The area with the maximal activation (ΔF/F 98th percentile) was determined and considered as the sensory core region. In order to investigate the biological significance of the previously identified components, an overlay of somatosensory components and the sensory core region was created (**Figure 19b**). This analysis

revealed a good spatial overlap of IVA retrieved components and stimulus-evoked brain activity. This allows attributing real functional relevance to the components identified by IVA.

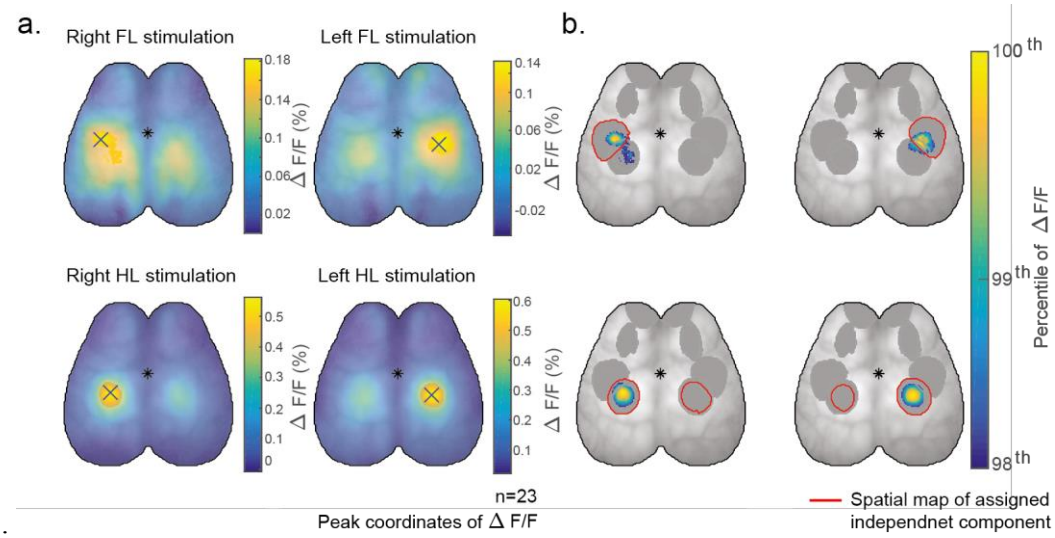

Figure 19: Topographical depiction of stimulus-evoked brain activity matches spatial maps of IVA. a. *Spatial maps of mean ΔF/F of 23 mice of stimulus evoked brain activity for each paw respectively (right and left forelimb (FL) and right and left hindlimb (HL))* ***b.*** *Overlay of the areas identified by IVA (grey), the 98th percentile of mean stimulation data (colour coded), and assigned component (red). The star locates bregma as a spatial reference in both a and b.*

These results suggest that the unbiased identification of anatomically distinct cortical areas with specific neurophysiological function can be accomplished by our IVA analysis pipeline.

3.3 Stroke

Finally, we aimed to investigate pathophysiological processes in brain disease using an experimental stroke model in mice. We wanted to investigate changes during the acute phase of a stroke in the motor cortex and assess recovery via functional connectivity analysis using widefield calcium imaging.

A photothrombotic lesion was induced in the motor cortex after determining its coordinates by ICA for each mouse (n=23) individually. In the control group sham surgery (n=17) was performed. Groups did not differ in weight at baseline (p=0.549). Functional imaging as well as behavioural assessment was conducted at baseline and on days 1, 3, 7, 14, 21, 28 and 56 after surgery.

Stroke induced an autofluorescent area in our imaging data which could potentially induce bias to our imaging analysis by generating artefacts. To eliminate this possibility, we intended to identify the infarct and assess size of the lesion using the data obtained from *in vivo* widefield calcium imaging. We detected a high correlation (R^2=0.704; p<0.0001; n=23) between the area of saturated pixels and the region of diminished blood-flow identified by laser speckle imaging on 1 day after surgery (**Figure 20**).

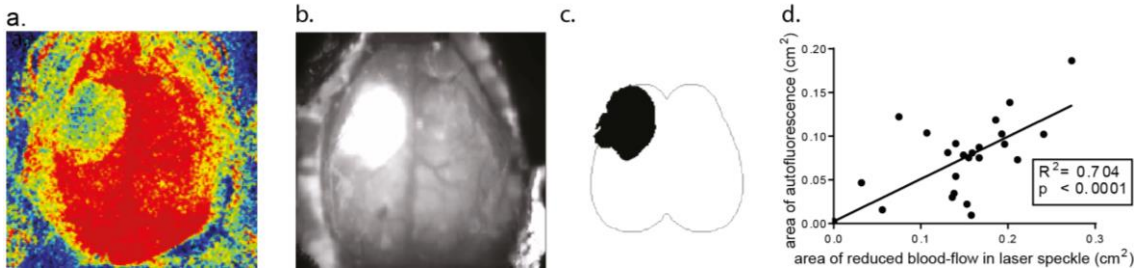

Figure 20: Autofluorescence in in vivo calcium imaging corresponds to area of cortical ischemia a. *Exemplary laser speckle image of a mouse cortex at D1 after stroke.* ***b.*** *One frame from calcium imaging of the same animal on D1. In the left motor cortex, autofluorescence induced by brain ischemia is clearly visible.* ***c.*** *Border of the general brain mask, applied to all recordings, and area of saturated pixel in black (originating from autofluorescence in panel b), which was subtracted from the general mask to generate an individual mask for this specific recording.* ***d.*** *Correlation between the areas of diminished blood flow assessed by laser speckle images and computed extent of saturated pixel in calcium imaging in 23 animals on the first after stroke. $R^2 = 0.704$ and $p<0.0001$*

This finding justifies the usage of cortical autofluorescence of necrotic brain tissue to define lesion size and location and with it their temporal evolution until 56 days after brain ischemia (**Figure 21**): After stroke we detected a large amount of autofluorescent pixels in the ischemic hemisphere. Later, long-term lesion involution could be observed by a decline in the autofluorescent area, resembling the necrotic brain tissue. We excluded saturated pixels from further analyses with the purpose of reducing possible imaging artefacts on the analysis.

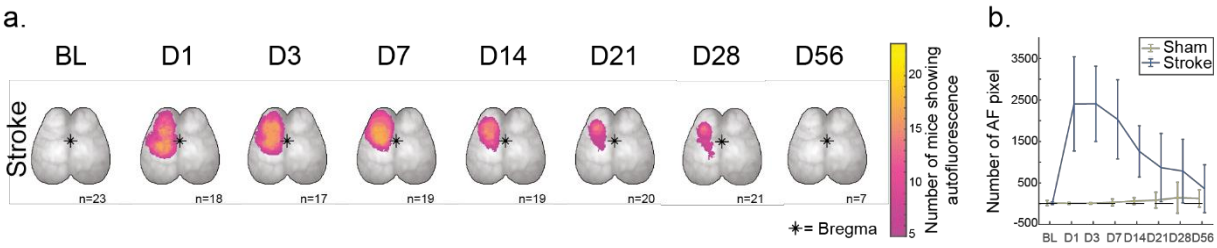

Figure 21: Evolution of stroke-induced autofluorescence over time. a*. Topographic depiction of autofluorescent pixel in stroke group for each acquisition time point.* ***b.*** *Quantification of autofluorescent pixel in in vivo calcium imaging in both groups over time.*

3.3.1 Impact of stroke on behaviour

We used two common behaviour tests to assess post-stroke motor deficits: The composite neuroscore and the beamwalk test (**Figure 22; Table 2**). Especially in the first 1-7 days after stroke, motor function was apparently impaired. The deficits were clearly detectable in both assessments the neuroscore and the beamwalk test. Later, neuroscore still identified significant behavioural limitations. Yet, while in the acute phase these deficits still improved over time, 2-way ANOVA analysis revealed a recovery plateau from day 7 to 56 as no significant improvements were present in between these days within the stroke group (Table 2). No significant deficits were observed in the beamwalk test later than 14 days post stroke.

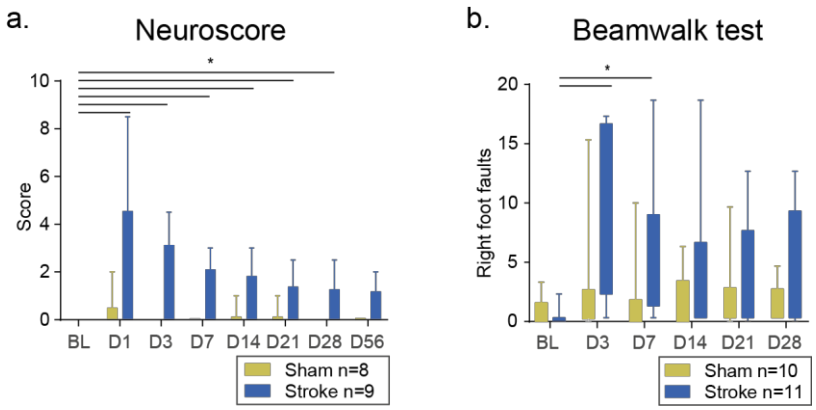

Figure 22: Stroke induced behavioural deficits assessed by neuroscore and beamwalk test. a. *Results of composed neuroscore of 15 sub-assessments to examine both global and focal deficits. A higher score mirroring worse deficits (sham: n=8, stroke: n=9).* ***b.*** *Results of beamwalk test counting right foot faults (sham: n=10, stroke: n=11). Statistical values have been obtained by repeated measure 2 way-ANOVA, *= p<0.05.; for more details see Table 2.*

Table 2: Results of repeated measure 2-way ANOVA of neuroscore data.

COMPARISON	SHAM	p-value	STROKE	p-value
Baseline vs. D1	ns	0.9976	****	<0.0001
Baseline vs. D3	ns	>0.9999	****	<0.0001
Baseline vs. D7	ns	>0.9999	****	<0.0001
Baseline vs. D14	ns	>0.9999	****	<0.0001
Baseline vs. D21	ns	>0.9999	**	0.0057
Baseline vs. D28	ns	>0.9999	*	0.0165
Baseline vs. D56	ns	>0.9999	ns	0.0713
D1 vs. D3	ns	0.9976	***	0.0003
D1 vs. D7	ns	0.9997	****	<0.0001
D1 vs. D14	ns	>0.9999	****	<0.0001
D1 vs. D21	ns	>0.9999	****	<0.0001
D1 vs. D28	ns	0.9976	****	<0.0001
D1 vs. D56	ns	0.9997	****	<0.0001
D3 vs. D7	ns	>0.9999	ns	0.6131
D3 vs. D14	ns	>0.9999	ns	0.1113
D3 vs. D21	ns	>0.9999	**	0.0018
D3 vs. D28	ns	>0.9999	***	0.0006
D3 vs. D56	ns	>0.9999	****	<0.0001
D7 vs. D14	ns	>0.9999	ns	>0.9999
D7 vs. D21	ns	>0.9999	ns	0.7465
D7 vs. D28	ns	>0.9999	ns	0.4761
D7 vs. D56	ns	>0.9999	ns	0.1689

D14 vs. D21	ns	>0.9999	ns	0.9991
D14 vs. D28	ns	>0.9999	ns	0.9773
D14 vs. D56	ns	>0.9999	ns	0.7465
D21 vs. D28	ns	>0.9999	ns	>0.9999
D21 vs. D56	ns	>0.9999	ns	>0.9999
D28 vs. D56	ns	>0.9999	ns	>0.9999

3.3.2 Impact of stroke on functional connectivity

To assess changes of network integrity in the acute and chronic phase after stroke in the motor cortex we acquired resting state imaging data. Consequently, functional connectivity was computed according to the protocol consolidated in the anaesthesia and network sub-studies. By tracing alterations of connectivity scores both, the acute pathological changes as well as the subsequent recovery of network function, could be investigated.

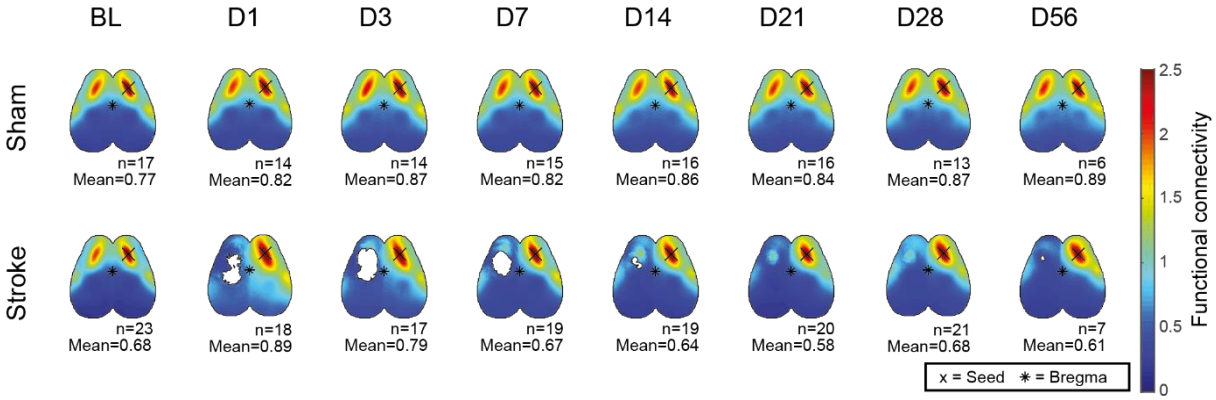

Figure 23: Changes in seed-based functional connectivity in sham and stroke animals after stroke. *Topographical depiction of seed-based functional connectivity with the reference ROI placed contralateral to the stroke in right caudal forelimb (rCFL). Connectivity scores are averaged for each acquisition day for stroke and sham group respectively (BL: baseline; D1-D56: days 1-56 after surgery). Black X indicates seed location, * indicates bregma as a reference.*

We detected a strong interhemispheric connectivity at baseline (naïve animals) between homotypic areas of both hemispheres (compare to Figure 14 and BL images **Figure 23 and Figure 24**). In accordance with previous studies, interhemispheric connectivity was dominantly characterizing the naïve brain network[58]. Given the strong connectivity between the motor cortices, we chose a ROI assigned to the structurally intact motor cortex (right caudal forelimb, rCFL) in the right hemisphere as the seed in seed-based functional connectivity analysis (**Figure 23**). Stroke affected mainly the interhemispheric connections which resulted in massively reduced functional connectivity scores between the rCFL and the infarcted hemisphere. This reduction continued for the entire follow-up period until day 56 post stroke. In contrast, the intrahemispheric functional connectivity of the contralesional hemisphere appeared only moderately altered after stroke.

In a second step, we aimed to investigate the changes specifically in the motor and sensory system to characterize the impact of an acute ischemic lesion within it. We addressed this by calculating ROI pair-wise functional connectivity. Here, we selected 8 (4 in each hemisphere) ROIs, which were retrieved by former group-IVA, within the sensorimotor cortex: RFL, CFL, FLs and HLs (see Results, second section, Figure 16b and Figure 17). In line with the findings of the seed-based analysis, ROI pair-wise analysis revealed strongly diminished functional connectivity from all analysed ROIs to the infarcted area and consequently a highly disturbed network function (Figure 24).

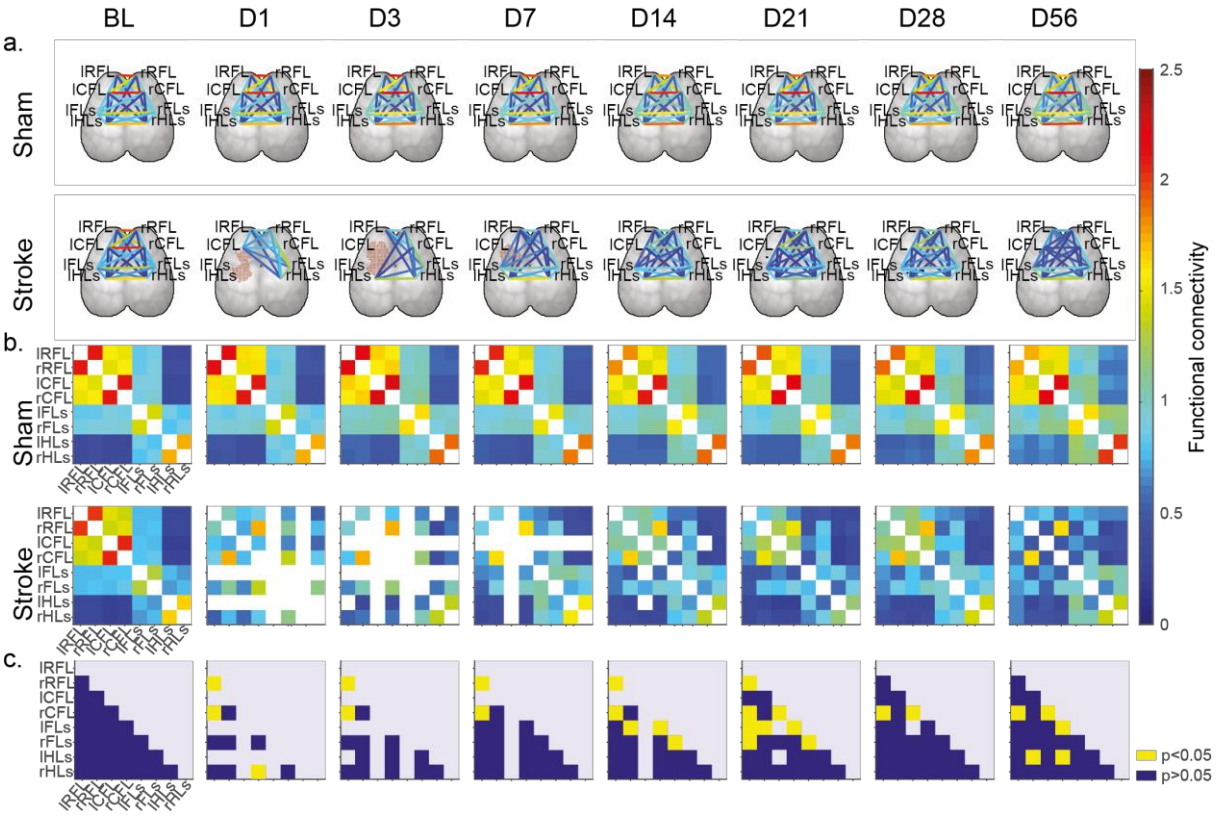

Figure 24: Changes in ROI pair-wise functional connectivity after stroke. *Each column in panels* ***a.*** *and* ***b****.: Group wise averaged functional connectivity scores are presented as* ***a.*** *graph and* ***b.*** *matrix for each day respectively (BL: baseline; D1-D56: days 1-56 after surgery). ROI pair-wise functional connectivity was calculated for 8 ROI, 4 in each hemisphere. Preselected ROI (identified by IVA) are located in rostral forelimb (RFL), caudal forelimb (CFL), hindlimb sensory (HLs) and forelimb sensory (FLs) areas, r and l refer to right or left hemisphere respectively. Functional connectivity scores are depicted as Fisher z-transformed Pearson's correlation; connections which involve less than 5 data points are not depicted (empty squares). * indicates bregma.* ***c.*** *Statistical results of comparison between sham and stroke for each acquisition time point are displayed as a matrix; p values attaint by two-sample t test were corrected via Bonferroni correction for multiple testing. Yellow squares indicate a significant group difference (p-corrected<0.05).*

Of note, not only the infarcted motor cortex but also the structurally unaffected part of the motor cortex more rostral to the lesion (RFL=rostral forelimb motor cortex) presented with reduced interhemispheric homotypic functional connectivity for at least 21 days after stroke. In comparison, the same interhemispheric homotypic functional connectivity of the somatosensory –located at comparable distance more caudal to the lesion core—was rather unaffected by the stroke (**Figure 25a,**

b). This discrepancy suggests a relatively distinct impact of the motoric lesion on the functionally dependent motor network rather than spatially neighboured areas.

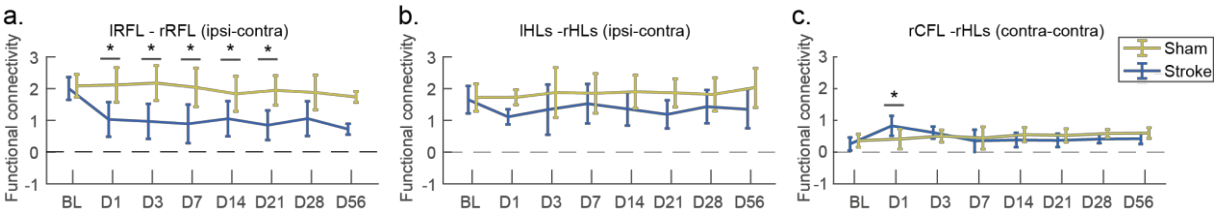

Figure 25: Functional connectivity of selected ROI pairs demonstrate strong affection of functionally dependent cortical areas after motor cortex lesion. a. *to* ***c.*** *Depiction of functional connectivity scores between* ***a.*** *left and right rostral forelimb (RFL: motor-motor interhemispheric),* ***b.*** *left and right hindlimb sensory (HLs: sensory-sensory interhemispheric) and* ***c.*** *right caudal forelimb (rCFL) and right HLs (motor-sensory, contralateral, intrahemispheric). Mean and standard deviation are displayed per group; significance bars indicate p-corrected<0.05.*

3.3.2.1 Impact of stroke on functional connectivity during the acute phase

Focusing on the temporal evolution of alterations in functional connectivity scores we detected changes specific to the acute phase after stroke. First, we detected transient higher functional connectivity scores in the acute phase after ischemic lesion in the structurally intact contralateral hemisphere. This increase normalized to baseline values already three days after stroke (**Figure 25c**).

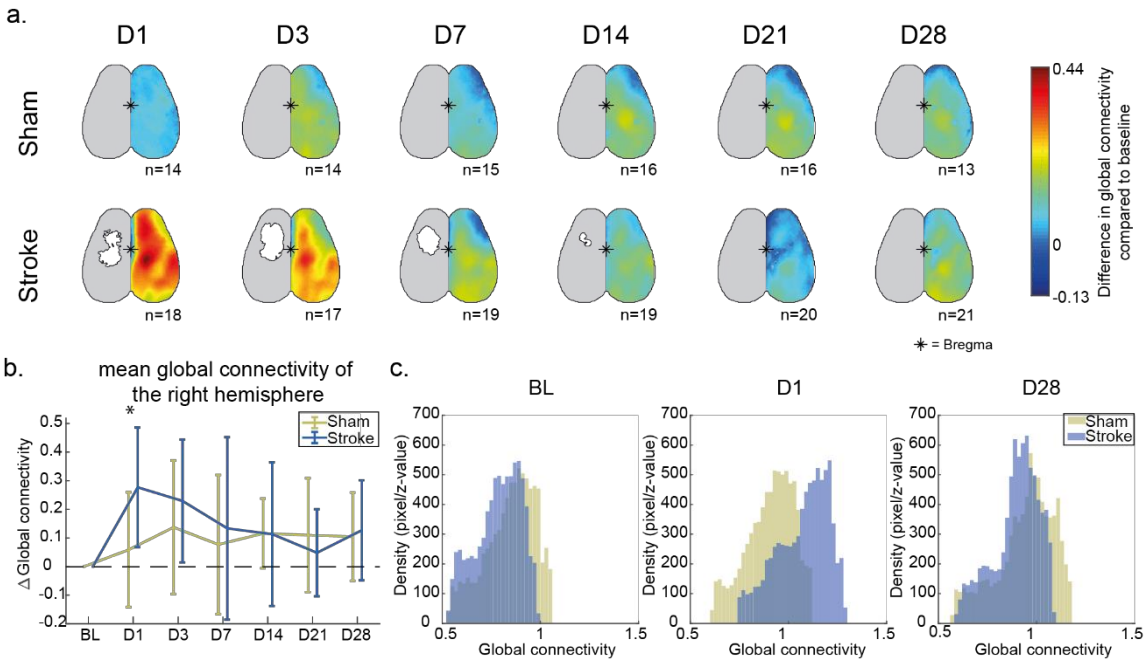

Figure 26: Changes in global connectivity of the contralateral hemisphere after stroke. a. *Topographical depiction of the mean alteration in global connectivity after photothrombosis (D1-D28: days 1-28 after surgery) for each pixel in the contralateral hemisphere separately. Global connectivity was normalized by subtracting each pixel the baseline global connectivity values from the corresponding pixel at each time point.* ***b.*** *Contralateral global connectivity normalized to baseline for each mouse. Mean and standard deviation are depicted until 28 days after photothrombosis. Significance bar indicates group differences with p-corrected < 0.05.* ***c.*** *Global connectivity of the right hemisphere depicted as a histogram for three time points (Baseline, Day 1 and Day 28). Mean of global connectivity values was computed per pixel, across the*

mice within stroke and sham group. The stroke group presents with significant increase global connectivity scores in the contralateral hemisphere when compared to sham, on the first day after stroke.

We used global connectivity analysis to investigate this acute consequence of the stroke within the contralateral hemisphere in an unbiased approach. This analysis allows assessing the more global effect of the acute brain injury on cortical network integrity. Global connectivity ascertains the overall functional connectivity of each pixel within a defined cortical region relative to all other pixels[55,56]. Here, we limited the masked area to the contralateral hemisphere to examine the impact of acute injury only in this remote non-lesioned area of the brain. In line with our other findings a significant transient increase in global connectivity could be detected on the first day after stroke. In resemblance with the results of the ROI pair-wise analysis especially areas within the sensorimotor system presented raised global connectivity values. At later days global connectivity scores declined to sham level (**Figure 26**).

We identified a second transient effect within the contralateral hemispheres. The area of very high functional connectivity values within the contralateral motor cortex values appeared larger in the acute phase after stroke in seed-based analysis (Figure 23, **Figure 27a**). In order to quantify this observation, the size of the structurally intact contralateral motor cortex was determined by extracting all pixels with greater connectivity value than 2.25. The number of identified pixels defined the size of the motor cortex. After stroke, we observed indeed a transient significant growth of contralateral motor area in stroke group whilst sham group remained unaffected. The size of the contralateral motor cortex normalized to levels of sham group on day three after stroke (**Figure 27**).

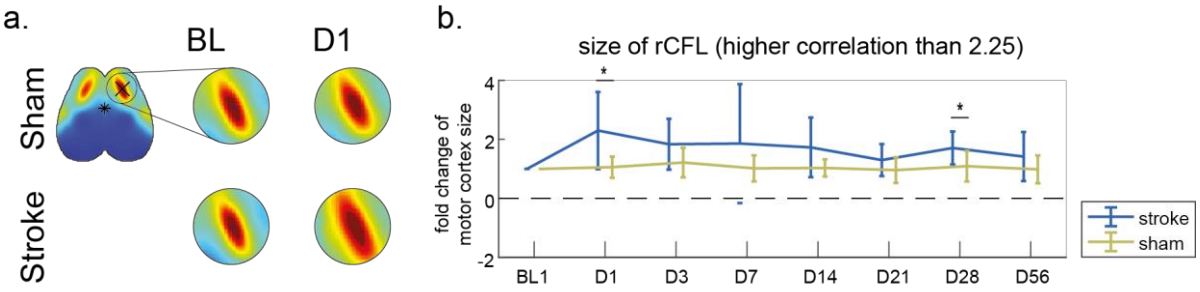

Figure 27: Size of the contralateral motor cortex increases significantly after stroke. a. *Magnification of seed-based functional connectivity analysis of sham and stroke group for baseline (BL) and 1 day after stroke (D1).* ***b.*** *Fold change of the contralateral motor cortex size approximated as number of pixels with higher functional connectivity scores than 2.25. Number of pixels is normalized to baseline. Two-sided t test with Bonferroni correction; significance bars indicate p-corrected < 0.05.*

3.3.2.2 Correlation of functional connectivity and behavioural outcome

To link behavioural outcome and functional connectivity we correlated the size of the contralateral motor cortex and behavioural outcome of the neuroscore test. The increase in contralateral motor size was associated with strong behaviour deficits detected in the neuroscore test (**Figure 28**) and

normalization preceding the recovery plateau from day 7 onwards, where no statistically improvement of the neuroscore could be detected anymore. Additionally, normalization of the interhemispheric functional connectivity scores of the RFL areas (Figure 25a) was temporally linked to the recovery plateau detected by neuroscore assessment (Figure 22a).

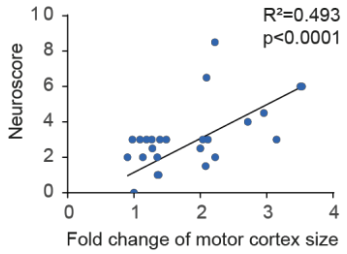

Figure 28: Increase in motor cortex size is associated with stronger behavioural deficits. *Correlation between fold change of contralateral motor cortex size and behavioural deficits detected by neuroscore. R^2=0.493; p<0.001*

In total, a complex pattern of alterations in connectivity scores characterizes the temporal evolution of brain networks after stroke: An acute increase in contralateral functional connectivity measures, a partial reformation of connectivity in some areas of the brain, uninfluenced connectivity within functionally more independent network components such as the sensory system, and at the same time preserved chronic reduction in connectivity to the primarily injured cortex area (i.e. lCFL). The association of functional connectivity values und behavioural assessments reveal high relevance of this imaging method to evaluate the functional outcome in preclinical stroke research.

4 Discussion

Preclinical research often lacks methods to assess meaningful translational outcome which might be the reason why most of the experimentally developed therapeutic treatments become lost in translation to clinical praxis[9,23,59]. We approached this problem by advancing *in vivo* widefield calcium imaging a method to measure brain activity and to investigate the impact of brain disease on functional neural networks in transgenic animals. The results confirm our tool –the conjunction of a rigorous sedation protocol and an analysis pipeline based on human fMRI analysis— to be a highly sensitive and reproducible method to investigate complex changes in cortical functional connectivity after stroke. The application of our approach in post-stroke recovery complements conventional readouts of experimental stroke such as behaviour testing in a meaningful manner and allows investigating brain function directly and repetitively *in vivo*.

4.1 *In vivo* widefield calcium imaging as a bedside-to-bench approach

Currently, the analysis of brain function plays a major role in clinical neuroscience. With the help of electroencephalography (EEG) and fMRI, physiology and pathophysiology of the brain has been, is and will be investigated. These key methods of modern neuroscience not only allow assessing brain function *in vivo* but are also implemented in daily clinical routine. Regarding the fact that most of the therapeutic approaches established in experimental research fail to show evidence in clinical trials[22], novel strategies in experimental design are urgently sought for. A currently still widely neglected approach is to maximize comparability of the outcome evaluation[24–26]. Given the importance of assessment of brain function in clinical neuroscience, an equivalent translational method is decisive to gain comparable readouts of therapeutic intervention in experimental research. However, the few options to investigate brain function in mice are currently unsatisfactory. Existing techniques need improvement especially regarding simple, daily and repetitive usage. Additionally, the implementation of advanced analysis strategies to existing methods is necessary for comparability to clinical research. In a reverse bedside-to-bench approach, we advanced the technique of *in vivo* calcium imaging[44,60] and applied classical algorithms used in fMRI and EEG analysis to introduce a modality for characterization of complex functional networks to translational neuroscience. Though being restricted to acquire only cortical information, *in vivo* widefield calcium imaging provides better spatial and temporal resolution compared to fMRI[61,62]. Moreover, high reproducibility and low stress levels for the animals due to a short procedure time are advantages of this modality and additionally at a reasonable price in comparison to fMRI. Our tool provides three major improvements compared to similar methods of *in vivo* calcium imaging[44,60,63–66]: Firstly, a stringent anaesthesia protocol resulting in minimal sedation to assure reproducible imaging conditions. In contrast, Silasi et al.[44], Wright et al.[65], Ma et al.[66] and others demonstrate awake imaging is definitely possible. Though, awake imaging would be preferable as the experimental set-up would resemble human stroke studies, we decided to

use anaesthetics. Nevertheless, we investigated the effect of anaesthesia thoroughly and demonstrated major differences in functional connectivity on resting state data between 1.0% ISO and 1.5% ISO, a range of concentration used for example in two similar studies[60,64]. However, in these studies[60,64] mainly stimulation-evoked brain activity was recorded for which we did not investigate the effect of anaesthesia which is likely not to be as profound. We accounted for this effect and established a rigorous protocol to diminish its effects on imaging data. Secondly, we designed a progressive analysis pipeline including an independent component analysis (ICA) to identify cortical networks for subsequent functional connectivity analysis. These advanced analysis strategies are important to allow translation to clinical studies[27]. We demonstrated the ROIs identified by ICA reflect distinct functional brain regions. In comparison, some studies use coordinates from an anatomical atlas for ROI definition[65], some use coordinates revealed by an iterative parcellation algorithm based on functional connectivity, where functionally clustered brain regions are grouped by an iterative process[63,67]. The third advantage is the solid intraindividual –over time— and interindividual –within the group— comparability provided by spatial alignment of all recordings. In comparison, comparability of functional connectivity analysis is based on bregma[65] or anatomical landmarks such as vessels[63] or not reported in detail so comparison to our approach is difficult. The two-step registration we use, is exceeding the reported methods by an exact intraindividual overlay of the recordings preceding the registration via anatomical landmarks for interindividual comparison which is comparable to the mentioned protocols. Together, these substantial enhancements over previously established, similar methods of *in vivo* widefield calcium imaging[44,60,63–66] are crucial to establish unprecedented comparability of the analysis of brain activity between men and mice.

4.2 Widefield calcium imaging and other imaging modalities

In vivo widefield calcium imaging is a novel approach in preclinical neuroscience. Yet, it is not the only option to perform functional imaging of brain activity in rodents. There have been numerous other imaging modalities established in animal research such as intrinsic optical imaging, fMRI, two-photon imaging and positron-emission tomography (PET). Just as *in vivo* widefield calcium imaging, all those modalities come with advantages and disadvantages over the others.

Intrinsic signal optical imaging is a method which uses the optical characteristics and alterations of the absorption spectrum of oxygenated blood and tissue[68]. This method uses a similar camera system than *in vivo* widefield calcium imaging but can be performed in wild-type mice. According to this, intrinsic optical imaging can be easily performed in any animal model of disease without elaborate crossbreeding beforehand. However, due to the expression of GCaMP protein in pyramidal neurons and its strong changes in fluorescence intensity during neural activity, *in vivo* widefield calcium imaging comes with a higher signal-to-noise ratio. This strong signal in *in vivo* widefield calcium imaging increases imaging quality undoubtedly. Additionally, in *in vivo* widefield calcium imaging neural activity can be measured directly and not only the surrogate parameters oxygenation status of

the blood and blood flow. With high signal-to-noise ratio and specific neural information, which is acquired, *in vivo* widefield calcium imaging clearly exceeds intrinsic optical imaging.

Two-photon imaging on the other hand is mostly performed on transgenic animals expressing genetically encoded calcium indicators (GECIs) as well but on a two-photon imaging system. This imaging modality presents with high resolution at the expense of only acquiring a very small cortical area including up to hundreds of neurons[69]. On the contrary, the holistic approach of *in vivo* widefield calcium imaging can assess brain activity of the entire forebrain cortex, while losing single cell resolution. With widefield calcium imaging a more differentiated analysis of spatially remote functional domains within the cortex can be performed beyond local microscale networks as in commonly used two-photon imaging. Additionally, two-photon imaging requires an invasive craniotomy and subsequent implantation of a cranial window. In *in vivo* widefield calcium there is no need for cranial trepanation which cannot be ruled out to affect brain function. In total, the two methods, *in vivo* widefield calcium imaging and two-photon imaging can be viewed as more complementary in nature rather than being alternative options with the former revealing a large-scale overview of functional brain networks and the latter adding microscale architectural information to it.

fMRI and PET are two very frequently use methods in human neuroscience research, hence with the greatest potential to be translational. However, these methods are still technically very challenging to be performed in rodents and especially small mice, let alone the costs and complexity of such a setup[70,71]. Both fMRI and PET are 3-dimensional imaging modalities which allow for an assessment of the entire brain function. In *in vivo* widefield calcium imaging only 2-dimensional imaging is currently possible and hence only cortical neural activity can be monitored. Certainly, the assessment of entire brain function is a major advantage nevertheless in both modalities spatial and temporal resolution (e.g. 0.5x0.5x10mm^3/voxel; 1Hz on a 4.7T scanner[61]) is quite limited and of minimum factor 10 below *in vivo* widefield calcium imaging (0.04x0.04mm^2/pixel; 25Hz). Additionally, both modalities are very time-consuming. Therefore, anaesthesia time and depth have to be expanded (25-46 min/per acquisition at least[61,62,72]) to conduct both fMRI and PET which we proved to crucially affect neural function. Here, feasibility of performing high resolution functional imaging on a daily base, with low stress levels to the animals due to short procedure time favours *in vivo* widefield calcium imaging.

Overall, *in vivo* widefield calcium imaging complements existing imaging options. It comes with both advantages and disadvantages. Unfortunately, *in vivo* widefield calcium imaging allows the assessment of cortical brain activity only, so investigation on the brain activity in central brain areas is not possible. Additionally, as being based on a transgenic mouse strains, extensive crossbreeding might be necessary for the investigation of some brain diseases. On the other hand, this method partly exceeds methods such as intrinsic optical imaging regarding signal-to-noise ratio, two-photon imaging regarding the assessment of wide parts of the cortex and 3-dimensional techniques regarding technical

feasibility. Therefore *in vivo* widefield calcium imaging is presenting itself as a promising technique to routinely investigate functional brain connectivity in mice[44,60,63–66].

4.3 Neurovascular coupling in imaging modalities

Physiologically, blood flow regulation and neural activity in the brain are tightly interconnected by a process termed neurovascular coupling. This complex process involves neurons, glia and vascular cells[73,74]. In brain diseases such as stroke and Alzheimer's disease, this multicellular process can be disturbed[73,75]. As fMRI and intrinsic optical imaging –blood-flow dependent imaging modalities– are based on neurovascular coupling to draw conclusion of brain activity, impairment of this process challenges the validity of interpretation on neural activity. *In vivo* widefield calcium imaging assesses neural activity directly via intensity changes of the GCaMP signal in pyramidal neurons and is therefore mostly independent of blood flow. This allows for investigation of functional neuronal networks in brain diseases which are known to influence neurovascular coupling. In addition, we show GCaMP signal is dominating the acquired data, so potential effects of hemodynamic absorption should be minimal. Unfortunately, in our set-up, parallel assessment of hemodynamic changes and calcium signal is not possible, which partially limits the statement of no interference of hemodynamic changes in our data. This potential impact of hemodynamic absorption on GCaMP signal has been previously described and would make simultaneous recording of both preferable in order to correct for potential interaction[65,76]. Additionally, a combined imaging modality which would allow the assessment of neuronal activity and blood-flow in parallel could reveal tremendous insights in the pathophysiology of neurovascular coupling and advance our knowledge of various brain diseases which are known to be tightly connected to this complex process.

4.4 Controlling the effect of anaesthesia on imaging data

One major consideration for the design of our method was to create a widely applicable and relatively easy way to handle imaging procedure. In human neuroscience research patients are usually imaged in awake state. Awake imaging in mice is certainly possible[44,65]. However, it demands a complex fixation procedure with e.g. head-fixing screw to control the still high risk of motion artefacts in imaging data[44]. Additionally, it requires investing a great amount of time to habituate mice to the imaging conditions. Concerning these factors, we rejected the option of awake imaging in the first place. Hence, we decided to acquire data from anesthetized animals to achieve the objective of an easy-to-perform procedure. Given the fact that the usage of anaesthetics might restrict the comparability between human and animal data, the reduction of its impact was one of our most pressing concerns. In fact, neuronal activity is affected by anaesthesia. Greater depth of anaesthesia results in frequency reduction and amplitude magnification of brain activity[77]. Readouts of functional imaging can be disturbed by this effect. Apparently, imaging parameters were highly prone to be affected by the depth of anaesthesia which we recognized during the process of establishing an appropriate sedation

protocol. Though some previous studies have demonstrated comparable results of awake and anesthetized animals during *in vivo* calcium imaging[44,78], we registered profound interaction of the depth of anaesthesia on brain function, frequency-based parameters and functional connectivity. To control this effect, different surrogate parameters of anaesthesia were tested. One of these parameters is ApEn estimation, a measure of randomness and signal complexity[50]. In EEG recordings, ApEn is known to be influenced by anaesthesia during surgery[79–81]. Moreover, this parameter is demonstrated to perform equally well to monitor depth of anaesthesia in patients compared to the bispectral index –a parameter ubiquitously used in surgery settings[81,82]. We were able to demonstrate $ApEn_{max}$ of the signal time course being highly susceptible to our different anaesthesia protocols. Hence, we used $ApEn_{max}$ to achieve two goals. First, to choose an appropriate anaesthesia protocol which would affect the physiological randomness of brain activity the least. Therefore, we chose our MED+ISO protocol which resulted in only light sedation. This anaesthesia regime interfered only minimally with randomness and at the same time preserved high spectral edge frequency of the data which is another well-described measure of depth of anaesthesia[82–84]. Secondly, we utilized ApEn values as a threshold marker to control for depth of anaesthesia of every recording in the stroke study to exclude possible affected data. The importance of this experiment is to demonstrate potential effects of anaesthesia on imaging readout parameters which might be present in other imaging modalities which use anesthetized animals as well. This effect is however widely discussed and discrepantly stated in previous publications. Consistent with our results, some studies demonstrate a major impact of anaesthetics on functional connectivity[62,72,85,86]. Grandjean et al.[62] investigated the effected of several different anaesthetics as well as dose dependent effects in mice fMRI data. They state prevailed interhemispheric connectivity in lower dose medetomidine treatment, while higher dose diminished these interhemispheric signal correlations. This reversed effect might be due to a major difference in signal processing (i.e. global signal removal) which might especially remove the dominant high amplitude and low frequency signal changes we found in deeper anaesthesia. In line with our findings, Kalthoff et al.[72] demonstrate isoflurane anaesthesia in comparable concentration to our 1.5% ISO group results in globally elevated functional connectivity with low topical specificity and high amplitude low frequency dominating the signal. However, lower dose of isoflurane reveals more similar patterns of functional connectivity seen in awake imaging than α-chloralose or urethane[85]. Additionally, receptor density for certain anaesthetics in specific brain regions and hence a more pronounced effect in those must be taken into account[86]. This effect can be especially observed in 3D fMRI data and might be the cause of different results using different drugs. Yet, other groups state no significant effect of anaesthesia on imaging data[44,78]. The reason for this inconsistency might be due to several reasons. On the one hand, the imaging methods in the studies differed as well as the subsequent analysis pipeline (e.g. global signal removal). On the other hand, it is possible that the distinct imaging modalities come with different sensitivity to the effects which are related to the depth of anaesthesia. In our study, the impact was profound, and we therefore offer our standardized

protocol combined with the threshold marker ApEn to monitor the result. These two methods combined provide high reproducibility and are easy to conduct.

4.5 Localisation of functional ROIs to characterize cortical networks

In resting state analysis of human fMRI data, independent component analysis (ICA) is a frequently used method to characterize functional networks[87,88]. With this method independent components within a given data set can be identified. In our experiment ICA retrieved independent cortical areas within the imaged brain, where independent relates to the recorded signal time courses of each pixel. In our analysis pipeline, we used ICA to identify resting state networks accordingly. More specifically we used IVA a multivariate extension of ICA. Lee et al. introduced IVA as an alternative for group analysis which circumvents permutation ambiguity of ICA[51]. One advantage of using ICA for network identification is based on its independence of a priori definition of any model time course, any seed or any region of interest[54]. It is well-demonstrated and became common sense, that in human fMRI or EEG data networks identified by ICA during resting state analysis generally overlap with the active brain regions in task dependent imaging[43]. In rodent imaging on the contrary, we are the first to our knowledge to prove this paradigm being applicable. We validated cortical networks retrieved by ICA by demonstrating an overlap with the areas of responses evoked by sensory stimuli. Analogous to human findings, spatially overlapping results of ICA and stimulus-evoked brain activity suggest that predominantly cortical areas with significant somatosensory and motor function are being identified by the ICA algorithm. Additionally, we were able to assign each of the components a physiological brain functionality by comparison with the Paxinos brain atlas[57]. Current imaging methods commonly determine the ROI based on sensory stimulation or even use only coordinates retrieved from stereotactic brain atlases[60,61,89–91]. We preferred the usage of an objective method such as ICA to identify these regions instead of relying on third party data. ICA provides two major advantages: Firstly, functional brain areas can be identified and used as ROI. Secondly, determination of ROI and investigation of imaging derived readouts such as functional connectivity can be conducted in the identical *in vivo* experiment.

4.6 Quality management of functional imaging after stroke

In a final step, we chose to implement our functional imaging approach in a disease model of stroke to study changes in cortical connectome after ischemia of the motor cortex. Necrotic brain tissue of the stroke caused substantial autofluorescence in the ischemic core region. Size of the infarct-induced autofluorescent area correlated with the size of the area of diminished blood-flow identified by laser speckle flowmetry. The possible interference of this autofluorescence on signal quality of adjacent cortical areas is an important consideration we addressed in our analysis pipeline. All saturated pixels were identified and excluded from subsequent analysis in order to minimize the potential impact caused by this technical limitation. Additionally, in order to diminish the possible artefact in single

pixel time courses we used pooled ROIs. This will help to stabilize network analysis especially around the border zone of the infarct. On the other hand, the resulting information loss impedes the analysis of fine peri-lesional networks, which might be better investigated by a different imaging method with focus on microscale networks such as *in vivo* two-photon imaging. Hence, complementing our experiments with two-photon imaging of the peri-lesional cortex would be of great scientific interest. In total, masking areas with high possibility to create artefacts and pooling data to diminish noise of single pixel time course will guarantee imaging quality throughout the stroke study at the expense of losing information of peri-lesional cortical areas.

4.7 Alterations in functional connectivity after motor cortex ischemia

The effects of stroke were both transient and chronic as well as both inter- and intrahemispherically distributed. Starting with the transient changes, we demonstrate alterations in contralateral functional connectivity scores in the acute phase post stroke. The intrahemispheric functional connectivity – defined by the connection between motor and sensory cortex within the hemisphere contralateral to the stroke— was temporally increased. In addition, this contralateral hemisphere presented with a transient increase in global functional connectivity acutely after the ischemic infarct. We further demonstrated a transient increase in size of the contralateral motor cortex. These findings go in line with a previously published study on functional connectivity after stroke which was conducted in rats by using fMRI. Here, van Meer et al. revealed a transient increase of intrahemispheric functional connectivity between primary somatosensory and primary motor cortex in the contralesional hemisphere[61]. Among other causes, the reduction of interhemispheric inhibition is discussed to contribute to the increase of functional connectivity[92]. Additionally, an increase of contralesional primary motor excitability was prevalent in the first weeks after stroke in human patients[93]. Human stroke research revealed this pathophysiological enhancement of neural activity within the contralateral motor cortex correlated with restoration of motor function[92,94,95]. Ward et al. demonstrate recovery-related decreases in task-related brain activation especially in motor-related regions such as premotor and motor cortex in the contralesional hemisphere in a longitudinal fMRI study[96]. However, it is unclear whether this enhancement in contralateral functional connectivity is driving positive or negative influence on mechanisms of recovery[94]. In our study, normalization of all three measures – global connectivity, increased contralateral intrahemispheric functional connectivity and size of the rCFL— was temporally linked to a recovery plateau, which was determined by no further statistical improvements of the deficits assessed by the neuroscore. Altogether, the transient effects were predominantly located in the contralateral hemisphere. The analysis of the interhemispheric functional connectivity revealed strong connection of homotypic cortical areas in the healthy brain as previously reported[58]. After stroke, these strong connections were significantly disrupted, especially in the acute and subacute phase. This reduction in interhemispheric connectivity was limited however to the motor system whereas the somatosensory cortex was not affected in our experimental stroke model. In

accordance with this, a cortical lesion revealed comparable restricted alterations to functionally closely linked cortical areas in stimulus-evoked brain activity[97]. Interestingly, subcortical stroke is reported to yield a more extensive effect on remote functional systems such as both sensorimotor and visual systems[61]. There are multiple possible processes which might drive the desynchronization in brain activity which we measured by interhemispheric functional connectivity after stroke. The acute injury as well as first regenerative mechanism and even secondary degeneration due to acute neuronal damage after the lesion could be involved in disturbing synchronic brain activity[98]. Brain function is crucially relying on a finetuned synergy of excitation and inhibition. Acute tissue damage might therefore disrupt this balanced brain synchronicity. Supporting this theory, a decreased interhemispheric inhibition from lesioned to contralesional motor cortex together with an enhanced contralesional brain activity was prevalent in human stroke studies in the first weeks after lesion[93,99]. Chronic changes might disturb synchronic brain function as well. One year after stroke, Kuchcinski et al. report remote changes in thalamus which might reflect secondary degeneration and correlate with the patients stroke outcome[100]. In line with this we demonstrate the interhemispheric functional connectivity was only partially restored in the chronic phase. This restoration might be a correlate of the still ongoing reparation of bilateral brain interaction and therefore a marker of regeneration. This possibility is underlined by the fact that normalization of the interhemispheric functional connectivity and restoration of the contralateral motor cortex size is associated with improvement of behavioural deficits.

4.8 The role of behavioural assessment and its limitations

After stroke, behavioural assessment in rodents has various limitations. Although frequently used in research, behaviour testing provides often very general and sometimes unspecific readouts of neurological recovery[29,59,101]. This is due to two main reasons. On the one hand, there is an intrinsic limitation in reducing complex neurological deficits to a general and easy assessment. This is not only the case in small animals such as mice but already in human assessment of neurological deficits[102]. Neurological deficits caused by stroke can be very complex. Additionally, neurological physical examination is very complex and partially very dependent on patients as it relies on their ability to correctly report their symptoms (in e.g. sensory assessment). This poses already difficulties in designing general assessments and scores for human patients. In small animals this impact is even more prominent as the assessment takes place naturally only in an observing manner. This observing already limits the examination of several neurological readouts such as sensory assessment. Therefore, the assessment of complex neurological deficits in mice is very constrained.

On the other hand, conduction and interpretation of behavioural tests can be easily influenced and are crucially dependent on the experimenter[59]. When conducting behaviour tests in small rodents, there are numerous confounding variables to be aware of which possibly change the readout such as the time of day the assessment takes place, randomisation or exclusion of the animals, subtle changes in smell and

of course habituation to the experimental set-up[59]. These confounding variables can sure be limited by setting fixed parameters for the assessment but can never be ruled out entirely. As mentioned above, behaviour tests are only observing. This observation is conducted by an experimenter and is therefore subjective. This makes comparison of readouts in between different experimenter and different laboratories very difficult. Additionally, this subjectivity might cause biased readouts which again can be diminished by blinding the experimenter[103,104]. To account for all confounding variables in behavioural test is very difficult which make them vulnerable to bias.

However, behaviour tests are a widely established and indispensable methods in preclinical research[59]. Their usage in animal experiments offer important and translational experimental endpoints and are the only way to measure physical functional outcome. Accounting for all named difficulties behavioural tests are a valid translational tool to study neurological diseases including stroke. In our study, we conducted two different behavioural tests –neuroscore and beamwalk test— to monitor post-stroke deficits. In the acute phase, these behavioural tests appear to be useful to assess stroke related deficits. The incongruent results in the recovery phase could be due to multiple assumptions such as either partial rehabilitation or compensation or only different sensitivity in observing long-term regeneration. Insensitivity of behavioural testing in the chronic stages was previously reported and the need for methods to assess functional outcome in the later phase discussed[59]. The examination of the chronic phase is the most relevant for clinical studies which urges the need of a more sensitive alternative to assess regenerative processes *in vivo*. With widefield calcium imaging we aimed to provide such a complementary application.

Functional brain imaging offers an unbiased and sensitive option of assessing functional changes and recovery in brain disease. Furthermore, *in vivo* widefield calcium imaging provides the possibility of assessing nearly the entire forebrain cortex and hence allows for the analysis of different functional cortical systems within one recording. The readouts and their conclusions such as contribution of different functional cortical systems, their degree of involvement on regenerative processes and even potential transient compensatory mechanisms can lead subsequent deeper analysis in the determined functional systems.

4.9 Conclusion

In vivo widefield calcium imaging – advanced by a stringed experimental protocol and a complex analytical pipeline – is an easy-to-perform method for repetitive assessment of functional networks in mice. So far, this method allows for assessment of cortical information only. Especially the chosen algorithms analogous to human fMRI analysis create a heavily required comparability between mice and humans to advance translational neuroscience in both mechanistic studies and establishment of novel therapies. *In vivo* widefield calcium revealed imaging parameters such as functional connectivity being associated to clinical outcome after stroke. This underlines the relevance of this approach to improve experimental stroke research and possibly even preclinical neuroscience in general. With its

wide applicability, *in vivo* widefield calcium imaging has the potential to be a required tool to drive investigation and reveal novel insights into a wide range of brain diseases.

5 Summaries

5.1 Summary

Stroke is one of the leading causes of death and its prevalence is still raising with aging society in future. Despite its major impact, only two specific therapies are approved in clinical practice, today. Thus, hundreds of possible therapies were identified in experimental research, none of them has proven efficiency on human patients. To address this loss in translation from experimental research to clinical practise, several fronts can be scrutinized. Among several options, the establishment of translational methods to assess functional clinical outcome in preclinical research is inevitable. To approach this one option is to develop modalities of functional imaging of the brain activity. Functional brain imaging not only allows to assess translational parameters for functional regeneration after stroke but also to investigate pathophysiological mechanisms in the brain. Hence, the analysis of functional brain activity in experimental stroke research could both identify new therapeutic targets and validate their effectiveness by creating a translational read-out.

Functional brain imaging is a frequently used method which strongly advanced our knowledge in neuroscience and as well in human stroke research. Its aim in general is a better understanding of brain functions, identification of functionally connected brain regions and their dynamic changes under certain conditions. In stroke research, the dynamic changes of functional network and its association with regeneration is of major interest. To investigate functional brain activity, functional magnetic resonance imaging (fMRI) is predominantly used in human research. fMRI faces great technical challenges and essential limitations for use in small rodents such as laboratory mice which are the most frequently used animals to study brain disease. This is why there is interest and need for alternative imaging modalities in experimental research. To benefit of the insights from human research in experimental research, we adapted and evolved the imaging modality of *in vivo* widefield calcium imaging. This imaging modality is based on transgenic animals who permit to investigate brain activity directly via GCaMP fluorescence. GCaMP is a genetically encoded calcium sensor which is well-known to mirror calcium fluctuations during action potential and with this neuronal activity. Via a customized imaging system, it is possible to acquire cortical neuronal activity and analyse it with comparable methods as used in human brain research. Hence, this method allows the repetitive investigation of brain activity *in vivo* in a translational manner.

In three studies we adapted and enhanced existing protocols to establish a reliable transgenic approach to assess functional brain connectivity. In a first study, we investigated the effect of anaesthesia on brain function and characterized the relationship of different frequency-based imaging parameters, functional connectivity and depth of anaesthesia. Subsequently, we established a stringent protocol for light sedation which is easy to use and results in reproducible imaging parameters. In a second study, we identified functional brain areas by using independent vector analysis (IVA) on resting state

imaging data. Therefore, we validated the identified areas with help of an anatomical atlas and stimulus-evoked brain activity. This validation justifies the usage of our unbiasedly selected cortical areas as functional seeds. Finally, we implemented the assessment of functional connectivity values after stroke. In this third study, we investigated repetitively the changes in functional connectivity up to 56 days after an ischemic lesion in the motor cortex induced by a photothrombotic model. We demonstrate both acute and chronic effects of ischemia to cortical functional connectivity. In the acute phase on the first day after stroke we demonstrate transient increase in contralateral functional connectivity. A second transient effect is the increase in contralateral motor cortex size. Third, chronic reduction in interhemispheric functional connectivity is present only in functionally but not anatomically close regions of the brain. And last, changes in both functional connectivity values and the size of contralateral motor cortex size are associated with the deficits assessed by behavioural testing. Hence, the identified parameters are of major relevance for the clinical outcome. The results establish two major facts: preclinical investigation of brain function is possible on a routinely basis and adds additional insight on pathophysiological mechanisms in brain disease which are associated with behavioural outcome. Consequently, the application of this translational imaging modality will not only be of great interest to stroke research but also to several brain diseases where pathophysiological mechanisms still need to be elucidated.

5.2 Zusammenfassung

Schlaganfall ist eine der häufigsten Todesursachen weltweit und seine Prävalenz wird mit steigendem Altersdurchschnitt in der Gesellschaft auch in Zukunft weiter zu nehmen. Trotz der großen Relevanz sind bis heute nur zwei spezifische Therapien für Schlaganfall in der klinischen Praxis zugelassen. Denn obwohl in experimentellen Untersuchungen bereits Hunderte von möglichen Therapien identifiziert wurden, konnte keine ihre Wirksamkeit bei Patienten nachweisen. Um diesem Verlust der Translation der experimentellen Forschung zur klinischen Anwendbarkeit entgegenzuwirken, können mehrere Komponenten hinterfragt werden. Eine davon ist die Etablierung von translationalen Methoden in der präklinischen Forschung, um funktionelle Ergebnisse mit klinischer Relevanz zu erheben. Eine Möglichkeit, dies umzusetzen, ist die Entwicklung von funktioneller Bildgebung der Hirnaktivität. Mit deren Hilfe können nicht translationale Parameter der funktionellen Regeneration nach Schlaganfall gemessen, sondern auch pathophysiologische Mechanismen im Gehirn untersucht werden. Daher könnte die Analyse der Gehirnaktivität mittels funktioneller Bildgebung in der experimentellen Schlaganfallforschung sowohl neue therapeutische Ziele identifizieren als auch deren Wirksamkeit durch ein translationales Untersuchungsergebnis validieren.

Die funktionelle Bildgebung des Gehirns ist eine häufig angewandte Methode, welche unser Wissen in der Neurowissenschaft und damit auch in der humanen Schlaganfallforschung nachhaltig erweiterte. Allgemeines Ziel ist ein besseres Verständnis der Gehirnfunktion, die Identifizierung funktionell verbundener Hirnregionen und die Ermittlung dynamischer Veränderungen unter bestimmten Bedingungen. In der Schlaganfallforschung sind insbesondere die dynamischen Veränderungen der funktionellen Netzwerke und deren Zusammenhang mit der Regeneration von großem Interesse. Zur Untersuchung der funktionellen Hirnaktivität wird in der Humanforschung vorwiegend die funktionelle Magnetresonanztomographie (fMRT) eingesetzt. Jedoch bringt diese Methode große technische Herausforderungen und wesentliche Einschränkungen bei der Untersuchung kleiner Nagetiere wie Labormäuse mit sich, welche die am häufigsten zur Untersuchung von Gehirnerkrankungen verwendete Tierart ist. Aus diesem Grund ist die Entwicklung alternativer Bildgebungsmodalitäten in der experimentellen Forschung von großer Relevanz. Um die Erkenntnisse aus der Forschung am Menschen in der experimentellen Forschung zu nutzen, haben wir die *In-vivo*-Weitfeld-Calcium-Bildgebung modifiziert und weiterentwickelt. Diese Bildgebungsmodalität basiert auf transgenen Tieren, die es erlauben, die Hirnaktivität direkt über GCaMP-Fluoreszenz zu untersuchen. GCaMP ist ein genetisch codierter Kalziumsensor, welcher die Kalziumfluktuationen während des Aktionspotentials und somit die neuronale Aktivität widerspiegelt. Mithilfe eines speziell angefertigten Kamerasystems kann die kortikale neuronale Aktivität aufgezeichnet und später mit Methoden, die analog zu denen in der humanen Forschung stehen, ausgewertet werden. Dies ermöglicht die repetitive, translationale Untersuchung des Gehirns *in vivo*.

In drei Studien haben wir bestehende Methoden angepasst und verbessert, um einen zuverlässigen Ansatz zur Analyse der funktionellen Gehirnaktivität zu etablieren. In einer ersten Studie untersuchten wir den Einfluss der Anästhesie auf die Gehirnfunktion und charakterisierten die Beziehung zwischen verschiedenen frequenzbasierten Bildgebungsparametern, funktioneller Konnektivität und Narkosetiefe. Infolgedessen erstellten wir ein stringentes Protokoll für eine leichte Sedierung, das einfach anzuwenden ist und reproduzierbare Bildgebungsparameter liefert. In einer zweiten Studie identifizierten wir funktionelle Hirnregionen mithilfe einer unabhängigen Vektoranalyse (IVA) in Bildgebungsdaten des Ruhezustands (*resting state*). Anschließend validierten wir die identifizierten kortikalen Areale mithilfe eines anatomischen Atlas und der durch sensorische Elektrostimulationen evozierten Hirnaktivität (*stimulus-evoked brain activity*). Diese Validierung rechtfertigt die Verwendung der objektiv und ohne Bias identifizierten Areale als funktionale Seeds. Zuletzt führten wir eine Analyse der funktionalen Konnektivität nach Schlaganfall durch. In dieser dritten Studie untersuchten wir die Veränderungen der funktionellen Konnektivität repetitiv bis zu 56 Tage nach einer ischämischen Läsion im motorischen Kortex, welche durch eine Photothrombose induziert wurde. Wir fanden sowohl akute als auch chronische Auswirkungen von Ischämie auf die kortikale funktionelle Konnektivität. In der akuten Phase, am ersten Tag nach Schlaganfall, zeigte sich eine vorübergehende Zunahme der kontralateralen funktionellen Konnektivität. Ein zweiter transienter Effekt war die funktionelle Vergrößerung des kontralateralen motorischen Areales. Als drittes stellte sich eine chronische Reduktion der interhemisphärischen funktionellen Konnektivität ein, welche nur in funktionell- aber nicht anatomisch-benachbarten Regionen des Gehirns auftrat. Die beobachteten Veränderungen in der funktionalen Konnektivität korrelierten zeitlich mit den Verhaltenstests festgestellten Defiziten. Aus dieser Korrelation ergibt sich möglicherweise eine große Relevanz der erhobenen Parameter für das klinische Behandlungsergebnis. Zusammenfassend unterstreichen die Ergebnisse zwei wesentliche Tatsachen: Die experimentelle Untersuchung der Gehirnfunktion von Mäusen ist routinemäßig möglich und liefert zusätzliche Erkenntnisse über pathophysiologische Mechanismen bei Hirnerkrankungen, die mit dem klinischen Zustand zusammenhängen. Folglich wird die Anwendung dieser translationalen Bildgebungsmodalität nicht nur für die Schlaganfallforschung von größerem Interesse sein, sondern auch für die Erforschung verschiedener Gehirnerkrankungen, bei denen die pathophysiologischen Mechanismen noch aufgeklärt werden müssen.

6 References

1. Definition of stroke from WHO. Available at: http://www.who.int/topics/cerebrovascular_accident/en/. (Accessed: 1st August 2019)

2. WHO: The top 10 causes of death. *Global Health Estimates 2016: Deaths by Cause, Age, Sex* (2018). Available at: https://www.who.int/news-room/fact-sheets/detail/the-top-10-causes-of-death. (Accessed: 2nd August 2019)

3. Benjamin, E. J. *et al. Heart Disease and Stroke Statistics—2019 Update: A Report From the American Heart Association*. *Circulation* **139**, (2019).

4. Seattle, WA: Institute for Health Metrics and Evaluation (IHME), U. of W. 2016. Global Burden of Disease Study 2016 (GBD 2016) Incidence, Prevalence, and Years Lived with Disability 1990-2016 | GHDx. Available at: http://ghdx.healthdata.org/record/ihme-data/gbd-2016-incidence-prevalence-and-ylds-1990-2016. (Accessed: 15th August 2019)

5. Reeves, M. J. *et al.* Sex differences in stroke: epidemiology, clinical presentation, medical care, and outcomes. *Lancet Neurol* **7**, 915–926 (2008).

6. Ovbiagele, B. *et al.* Forecasting the future of stroke in the united states: A policy statement from the American heart association and American stroke association. *Stroke* **44**, 2361–2375 (2013).

7. Förch, C. & Neumann-Haefelin, T. The Projected Burden of Stroke in the German Federal State of Hesse up to the Year 2050: In Reply. *Dtsch. Aerzteblatt Internatiional* **105**, 467–473 (2008).

8. *Center of disease control and prevention: Prevalence and Most Common Causes of Disability Among Adults --- United States, 2005*. (2009). doi:58(16):421–426

9. Feigin, V. L. *et al.* Update on the Global Burden of Ischemic and Hemorrhagic Stroke in 1990-2013: The GBD 2013 Study. *Neuroepidemiology* **45**, 161–176 (2015).

10. Wilkins, E., L., W., Wickramasinghe, K. & P, B. European Cardiovascular Disease Statistics 2017 edition. *Eur. Hear. Netw.* 8–15; 94, 118, 127, 149, 162, 174 (2017).

11. World Health Organization. Global Health Estimates 2016: Deaths by Cause, Age, Sex, by Country and by Region, 2000-2016. (2018).

12. Sacco, R. L. *et al.* An updated definition of stroke for the 21st century: A statement for healthcare professionals from the American heart association/American stroke association. *Stroke* **44**, 2064–2089 (2013).

13. Adams, H. . *et al.* Classification of Subtype of Acute Ischemic Stroke. *Stroke* **23**, 35–41 (1993).

14. Vemmos, K. N. *et al.* The Athens Stroke Registry: Results of a Five-Year Hospital-Based Study. *Cerebrovasc. Dis.* **10**, 133–141 (2000).

15. Martí-Vilalta, J. L. & Arboix, A. The Barcelona Stroke Registry. *Eur. Neurol.* **41**, 135–142 (1999).

16. Woodruff, T. M. *et al.* Pathophysiology, treatment, and animal and cellular models of human ischemic stroke. *Mol. Neurodegener.* **6**, 1–19 (2011).

17. Broughton, B. R. S., Reutens, D. C. & Sobey, C. G. Apoptotic mechanisms after cerebral ischemia. *Stroke* **40**, (2009).

18. Powers, W. J. *et al. AHA / ASA Guideline 2018 Guidelines for the Early Management of Patients With Acute Ischemic Stroke*. (2018). doi:10.1161/STR.0000000000000158

19. The National Institute of Neurological Disorders and Stroke rt-PA Stroke Study Group. Tissue

Plasminogen Activator for Acute Ischemic Stroke. *N. Engl. J. Med.* **333**, 1581–1587 (1995).

20. Endres, M. *et al.* Arbeitsgemeinschaft der Wissenschaftlichen Medizinischen Fachgesellschaften. S3 Leitlinie: Sekundärprophylaxe ischämischer Schlaganfall und transitorische ischämische Attacke. *AWMF Leitlinie* **1**, 1–60 (2015).

21. Rinaldo, L., Cloft, H. J., Castilla, L. R., Rabinstein, A. A. & Brinjikji, W. Utilization rates of tissue plasminogen activator and mechanical thrombectomy in patients with acute stroke and underlying malignancy. *J. Neurointerv. Surg.* **11**, 768–771 (2019).

22. O'Collins, V. E. *et al.* 1,026 Experimental treatments in acute stroke. *Ann. Neurol.* **59**, 467–477 (2006).

23. Roth, S. & Liesz, A. Stroke research at the crossroads - where are we heading? *Swiss Med. Wkly.* **146**, (2016).

24. Dirnagl, U. & Fisher, M. International, multicenter randomized preclinical trials in translational stroke research: It's time to act. *J. Cereb. Blood Flow Metab.* **32**, 933–935 (2012).

25. Bath, P. M. W., Macleod, M. R. & Green, A. R. Emulating Multicentre Clinical Stroke Trials: A New Paradigm for Studying Novel Interventions in Experimental Models of Stroke. *Int. J. Stroke* **4**, 471–479 (2009).

26. Howells, D. W., Sena, E. S., O'Collins, V. & Macleod, M. R. Improving the Efficiency of the Development of Drugs for Stroke. *Int. J. Stroke* **7**, 371–377 (2012).

27. Corbett, D. *et al.* Enhancing the alignment of the preclinical and clinical stroke recovery research pipeline: Consensus-based core recommendations from the Stroke Recovery and Rehabilitation Roundtable translational working group. *Int. J. Stroke* **12**, 462–471 (2017).

28. Schallert, T., Fleming, S. M., Leasure, J. L., Tillerson, J. L. & Bland, S. T. CNS plasticity and assessment of forelimb sensorimotor outcome in unilateral rat models of stroke, cortical ablation, parkinsonism and spinal cord injury. *Neuropharmacology* **39**, 777–787 (2000).

29. Llovera, G. *et al.* Results of a preclinical randomized controlled multicenter trial (pRCT): Anti-CD49d treatment for acute brain ischemia. *Sci. Transl. Med* **7**, 1–10 (2015).

30. Dacosta-Aguayo, R. *et al.* Prognostic value of changes in resting-state functional connectivity patterns in cognitive recovery after stroke: A 3T fMRI pilot study. *Hum. Brain Mapp.* **35**, 3819–3831 (2014).

31. Norris, D. G. Principles of magnetic resonance assessment of brain function. *J. Magn. Reson. Imaging* **23**, 794–807 (2006).

32. Logothetis, N. K. What we can do and what we cannot do with fMRI. *Nature* **453**, 869–878 (2008).

33. Hillman, E. M. C. Coupling Mechanism and Significance of the BOLD Signal: A Status Report. *Annu. Rev. Neurosci.* **37**, 161–181 (2014).

34. Soares, J. M. *et al.* A Hitchhiker's guide to functional magnetic resonance imaging. *Front. Neurosci.* **10**, 1–35 (2016).

35. Sabatini, B. L., Oertner, T. G. & Svoboda, K. The Life Cycle of Ca 2 Ions in Dendritic Spines. *Neuron* **33**, 439–452 (2002).

36. Dana, H. *et al.* Thy1-GCaMP6 transgenic mice for neuronal population imaging in vivo. *PLoS One* **9**, 1–9 (2014).

37. Nakai, J., Ohkura, M. & Imoto, K. A high signal-to-noise Ca2+ probe composed of a single

green fluorescent protein. *Nat. Biotechnol.* **19**, 137–141 (2001).

38. Barnett, L. M., Hughes, T. E. & Drobizhev, M. Deciphering the molecular mechanism responsible for GCaMP6m's Ca2+-dependent change in fluorescence. *PLoS One* **12**, 1–24 (2017).

39. Pologruto, T. A., Yasuda, R. & Svoboda, K. Monitoring neural activity and [Ca2+] with genetically encoded Ca2+ indicators. *J. Neurosci.* **24**, 9572–9 (2004).

40. Chen, Q. *et al.* Imaging Neural Activity Using Thy1-GCaMP Transgenic Mice. *Neuron* **76**, 297–308 (2012).

41. Van Den Heuvel, M. P. & Pol, H. E. H. Exploring the brain network: A review on resting-state fMRI functional connectivity. *Psiquiatria Biologica* (2011). doi:10.1016/j.psiq.2011.05.001

42. Friston, K. J. Functional and Effective Connectivity: A Review. *Brain Connect.* **1**, 13–36 (2011).

43. Smith, S. M. *et al.* Correspondence of the brain's functional architecture during activation and rest. *PNAS* **106**, 13040–13045 (2009).

44. Silasi, G., Xiao, D., Vanni, M. P., Chen, A. C. N. & Murphy, T. H. Intact skull chronic windows for mesoscopic wide-field imaging in awake mice. *J. Neurosci. Methods* **267**, 141–149 (2016).

45. Schindelin, J., Rueden, C. T., Hiner, M. C. & Eliceiri, K. W. The ImageJ ecosystem: An open platform for biomedical image analysis. *Mol. Reprod. Dev.* **82**, 518–529 (2015).

46. Luong, T. N., Carlisle, H. J., Southwell, A. & Patterson, P. H. Assessment of Motor Balance and Coordination in Mice using the Balance Beam. *JoVE* **49**, (2011).

47. Orsini, F. *et al.* Targeting mannose-binding lectin confers long-lasting protection with a surprisingly wide therapeutic window in cerebral ischemia. *Circulation* **126**, 1484–1494 (2012).

48. Pincus, S. M. Approximate entropy as a measure of system complexity. *Mathematics* **88**, 2297–2301 (1991).

49. Lee, K. Fast Approximate Entropy. (2012).

50. Chon, K., Scully, C. & Lu, S. Approximate entropy for all signals. *IEEE Eng. Med. Biol. Mag.* **28**, 18–23 (2009).

51. Lee, I., Kim, T. & Lee, T.-W. Fast fixed-point independent vector analysis algorithms for convolutive blind source separation. *Signal Processing* **87**, 1859–1871 (2007).

52. Lee, J.-H., Lee, T.-W., Jolesz, F. A. & Yoo, S.-S. Independent vector analysis (IVA): Multivariate approach for fMRI group study. *Neuroimage* **40**, 86–109 (2008).

53. Hutchison, D. & Mitchell, J. C. *Latent Variable Analysis and Signal Separation*. (Springer, 2010).

54. Michael, A. M., Anderson, M., Miller, R. L., AdalÄ±, T. & Calhoun, V. D. Preserving subject variability in group fMRI analysis: performance evaluation of GICA vs. IVA. *Front. Syst. Neurosci.* **8**, 1–18 (2014).

55. Cole, M. W., Pathak, S. & Schneider, W. Identifying the brain's most globally connected regions. *Neuroimage* **49**, 3132–3148 (2010).

56. Rubinov, M. & Sporns, O. Weight-conserving characterization of complex functional brain networks. *Neuroimage* **56**, 2068–2079 (2011).

57. Franklin, K. B. J. & Paxinos, G. *The Mouse Brain in Stereotactic Coordinates Third Edition*. (Elsevier Inc., 2007).

58. Bauer, A. Q. *et al.* Optical imaging of disrupted functional connectivity following ischemic stroke in mice. *Neuroimage* **99**, 388–401 (2014).

59. Balkaya, M., Kröber, J. M., Rex, A. & Endres, M. Assessing post-stroke behavior in mouse models of focal ischemia. *J. Cereb. Blood Flow Metab.* **33**, 330–338 (2013).

60. Vanni, M. P. & Murphy, T. H. Mesoscale Transcranial Spontaneous Activity Mapping in GCaMP3 Transgenic Mice Reveals Extensive Reciprocal Connections between Areas of Somatomotor Cortex. *J. Neurosci.* **34(48)**, 15931–15946 (2014).

61. Van Meer, M. P. A. *et al.* Recovery of Sensorimotor Function after Experimental Stroke Correlates with Restoration of Resting-State Interhemispheric Functional Connectivity. *J. Neurosci.* **30(11)**, 3964–3972 (2010).

62. Grandjean, J., Schroeter, A., Batata, I. & Rudin, M. Optimization of anesthesia protocol for resting-state fMRI in mice based on differential effects of anesthetics on functional connectivity patterns. *Neuroimage* **102**, 838–847 (2014).

63. Matsui, T., Murakami, T. & Ohki, K. Transient neuronal coactivations embedded in globally propagating waves underlie resting-state functional connectivity. *Proc. Natl. Acad. Sci. U. S. A.* **113**, 6556–61 (2016).

64. Kozberg, M. G., Ma, Y., Shaik, M. A., Kim, S. H. & Hillman, E. M. C. Rapid Postnatal Expansion of Neural Networks Occurs in an Environment of Altered Neurovascular and Neurometabolic Coupling. *J. Neurosci.* **36**, 6704–6717 (2016).

65. Wright, P. W. *et al.* Functional connectivity structure of cortical calcium dynamics in anesthetized and awake mice. *PLoS One* **12**, e0185759 (2017).

66. Ma, Y. *et al.* Resting-state hemodynamics are spatiotemporally coupled to synchronized and symmetric neural activity in excitatory neurons. doi:10.1073/pnas.1525369113

67. White, B. R. *et al.* Imaging of functional connectivity in the mouse brain. *PLoS One* **6**, (2011).

68. Ying, M. *et al.* Wide-field optical mapping of neural activity and brain haemodynamics: considerations and novel approaches. *Philos. Trans. R. Soc. B Biol. Sci.* **371**, 20150360 (2016).

69. Göbel, W., Kampa, B. M. & Helmchen, F. Imaging cellular network dynamics in three dimensions using fast 3D laser scanning. *Nat. Methods* **4**, 73–79 (2007).

70. Schroeter, A., Schlegel, F., Seuwen, A., Grandjean, J. & Rudin, M. Specificity of stimulus-evoked fMRI responses in the mouse: The influence of systemic physiological changes associated with innocuous stimulation under four different anesthetics. *Neuroimage* **94**, 372–384 (2014).

71. Zerbi, V., Grandjean, J., Rudin, M. & Wenderoth, N. Mapping the mouse brain with rs-fMRI: An optimized pipeline for functional network identification. *Neuroimage* **123**, 11–21 (2015).

72. Kalthoff, D., Po, C., Wiedermann, D. & Hoehn, M. Reliability and spatial specificity of rat brain sensorimotor functional connectivity networks are superior under sedation compared with general anesthesia. *NMR Biomed.* **26**, 638–650 (2013).

73. Iadecola, C. Neurovascular regulation in the normal brain and in Alzheimer's disease. *Nat. Rev. Neurosci.* **5**, 347–360 (2004).

74. Lauritzern, M. J. Reading vascular changes in brain imaging: Is dendritic calcium the key? *J. Cereb. Blood Flow Metab.* **25**, S684–S684 (2005).

75. Balbi, M., Koide, M., Wellman, G. C. & Plesnila, N. Inversion of neurovascular coupling after subarachnoid hemorrhage in vivo. *J. Cereb. Blood Flow Metab.* **37**, 3625–3634 (2017).

76. Ma, Y. *et al.* Wide-field optical mapping of neural activity and brain haemodynamics: considerations and novel approaches. *Philos. Trans. R. Soc. Lond. B. Biol. Sci.* **371**, (2016).

77. Kiersey, D. K., Bickford, R. G. & Faulconer, A. Electro-encephalographic patterns produced by thiopental sodium during surgical operations: Description and classification. *Br. J. Anaesth.* **23**, 141–152 (1951).

78. Mohajerani, M. H., Mcvea, D. A., Fingas, M. & Murphy, T. H. Mirrored Bilateral Slow-Wave Cortical Activity within Local Circuits Revealed by Fast Bihemispheric Voltage-Sensitive Dye Imaging in Anesthetized and Awake Mice. *J. Neurosci.* **30(10)**, 3745–3751 (2010).

79. Liu, Q., Chen, Y.-F., Fan, S.-Z., Abbod, M. F. & Shieh, J.-S. A comparison of five different algorithms for EEG signal analysis in artifacts rejection for monitoring depth of anesthesia. *Biomed. Signal Process. Control* **25**, 24–34 (2016).

80. Bruhn, J., Rö, H. & Hoeft, A. *Approximate Entropy as an Electroencephalographic Measure of Anesthetic Drug Effect during Desflurane Anesthesia*. *Anesthesiology* **92**, (2000).

81. Bruhn, J. *et al.* Correlation of Approximate Entropy, Bispectral Index, and Spectral Edge Frequency 95 (SEF95) with Clinical Signs of "Anesthetic Depth" during Coadministration of Propofol and Remifentanil. *Anesthesiol. J. Am. Soc. Anesthesiol.* **98**, 621–627 (2003).

82. Bruhn, J., Myles, P. S., Sneyd, R. & Struys, M. M. R. F. Depth of anaesthesia monitoring: what's available, what's validated and what's next? *Br. J. Anaesth.* **97**, 85–94 (2006).

83. Katoh, T., Suzuki, A. & Ikeda, K. Electroencephalographic derivatives as a tool for predicting the depth of sedation and anesthesia induced by sevoflurane. *Anesthesiology* **88**, 642–650 (1998).

84. Drummond, J. C., Brann, C. A., Perkins, D. E. & Wolfe, D. E. A comparison of median frequency, spectral edge frequency, a frequency band power ratio, total power, and dominance shift in the determination of depth of anesthesia. *Acta Anaesthesiol. Scand.* **35**, 693–699 (1991).

85. Jonckers, E. *et al.* Different anesthesia regimes modulate the functional connectivity outcome in mice. *Magn. Reson. Med.* **72**, 1103–1112 (2014).

86. Nasrallah, F. A., Tay, H. C. & Chuang, K. H. Detection of functional connectivity in the resting mouse brain. *Neuroimage* **86**, 417–424 (2014).

87. McKeown, M. J. *et al.* Analysis of fMRI data by blind separation into independant spatial components. *Hum. Brain Mapp.* **6**, 160–188 (1998).

88. Calhoun, V. D., Adali, T., Pearlson, G. D. & Pekar, J. J. Functional neuroanatomy of visuo-spatial working memory in turner syndrome. *Hum. Brain Mapp.* **14**, 96–107 (2001).

89. Mcgirr, A. *et al.* Cortical functional hyperconnectivity in a mouse model of depression and selective network effects of ketamine-functional-hyperconnectivity-in-a-mouse. *BRAIN* **140**, 2210–2225 (2017).

90. Vanni, M. P., Chan, A. W., Balbi, M., Silasi, G. & Murphy, T. H. Mesoscale Mapping of Mouse Cortex Reveals Frequency-Dependent Cycling between Distinct Macroscale Functional Modules. *J. Neurosci.* **37**, 7513–7533 (2017).

91. Hakon, J. *et al.* Multisensory stimulation improves functional recovery and resting-state functional connectivity in the mouse brain after stroke. *NeuroImage Clin.* **17**, 717–730 (2018).

92. Grefkes, C. *et al.* Cortical connectivity after subcortical stroke assessed with functional magnetic resonance imaging. *Ann. Neurol.* **63**, 236–246 (2008).

93. Bütefisch, C. M., Weßling, M., Netz, J., Seitz, R. J. & Hömberg, V. Relationship between

interhemispheric inhibition and motor cortex excitability in subacute stroke patients. *Neurorehabil. Neural Repair* **22**, 4–21 (2008).

94. Grefkes, C. & Fink, G. R. Reorganization of cerebral networks after stroke: New insights from neuroimaging with connectivity approaches. *Brain* **134**, 1264–1276 (2011).

95. Rehme, A. K., Fink, G. R., Von Cramon, D. Y. & Grefkes, C. The role of the contralesional motor cortex for motor recovery in the early days after stroke assessed with longitudinal fMRI. *Cereb. Cortex* (2011). doi:10.1093/cercor/bhq140

96. Ward, N. S., Brown, M. M., Thompson, A. J. & Frackowiak, R. S. J. Neural correlates of motor recovery after stroke: a longitudinal fMRI study. *Brain* **126**, 2476–2496 (2003).

97. Lim, D. H., Ledue, J. M., Majid, X., Mohajerani, H. & Murphy, T. H. Optogenetic Mapping after Stroke Reveals Network-Wide Scaling of Functional Connections and Heterogeneous Recovery of the Peri-Infarct. *J. Neurosci.* **43(49)**, 16455–16466 (2014).

98. Duering, M. & Schmidt, R. Remote changes after ischaemic infarcts: a distant target for therapy? *Brain* **140**, 1818–1820 (2017).

99. Murase, N., Duque, J., Mazzocchio, R. & Cohen, L. G. Influence of Interhemispheric Interactions on Motor Function in Chronic Stroke. *Ann. Neurol.* **55**, 400–409 (2004).

100. Kuchcinski, G. *et al.* Thalamic alterations remote to infarct appear as focal iron accumulation and impact clinical outcome. *Brain* **140**, 1932–1946 (2017).

101. Trueman, R. C. *et al.* Systematic and detailed analysis of behavioural tests in the rat middle cerebral artery occlusion model of stroke: Tests for long-term assessment. *J. Cereb. Blood Flow Metab.* **37**, 1349–1361 (2017).

102. Harrison, J. K., McArthur, K. S. & Quinn, T. J. Assessment scales in stroke: Clinimetric and clinical considerations. *Clin. Interv. Aging* **8**, 201–211 (2013).

103. Macleod, M. R. *et al.* Good laboratory practice: preventing introduction of bias at the bench. *Stroke.* **40**, 50–52 (2009).

104. Altman, D., Schulz, K. & Moher, D. The Revised CONSORT Statemnt for Reporting Randomized Trials: Explanation and Elaboration. *Ann Intern Med.* **134**, 663–694 (2001).

7 List of Abbreviations

ApEn	Approximate Entropy
$ApEn_{max}$	Maximum approximate entropy
BOLD	Blood-oxygenation level dependent
CaM	Calmodulin
DALY	Disability-adjusted life-years
EEG	Electroencephalography
F	Fluorescence
FLs	Forelimb sensory
fMRI	Functional magnetic resonance imaging
GECI	Genetically encoded calcium sensor
GFP	Green fluorescent protein
GICA	Group independent component analysis
HLs	Hindlimb sensory
ICA	Independent component analysis
ISO	Isofluorane
IVA	Independent component analysis
LED	Light emitting diode
MED	Medetomidine
MF	Median frequency
MRI	Magnetic resonance imaging
PET	Positron-emission tomography
rCFL	Right caudal forelimb
RFL	Rostral Forelimb
ROI	Region of interest
SEF	Spectral edge frequency
Thy1-GCaMP	C57BL/6J-Tg(Thy1-GCaMP6s)GP4.12Dkim/J heterozygous mice
tPA	Tissue plasminogen activator
WHO	World health organisation

8 List of Tables and Figures

8.1 List of tables

8.2 List of figures

9 Acknowledgements / Danksagung

Ich möchte diese Gelegenheit zunächst nutzen, um meiner Mama und meiner Schwester, Andrea und Toni Cramer für ihre unermüdliche Unterstützung, Motivation und Verständnis sowohl während meiner gesamten Ausbildung und im Speziellen während dieser Doktorarbeit zu danken. Ohne euch wäre es nie so weit gekommen. Ich bin froh, dass ich euch habe. Kein geringerer Dank gilt meiner gesamten Familie. Der von euch gebotenen Rückzugsort und eure stetige Unterstützung gibt besonders in anstrengenden Momenten viel Halt.

Mein besonderer Dank gilt auch meinem Doktorvater PD Dr. Arthur Liesz, dessen Energie, Enthusiasmus und Leidenschaft für die Forschung ansteckend sind. Die Erfahrungen, die ich im Labor, auf Kongressen oder während der Lab-Meetings sammeln durfte, habe ich größtenteils ihm zu verdanken. Danke nicht nur für die Möglichkeit an diesem Projekt arbeiten zu dürfen, für Deine lenkenden Ratschläge und für jederzeit mögliche Diskussion, sondern auch deine Beharrlichkeit auf Struktur, Präzision und Präsentation von welcher ich sicherlich für mein restliches Leben profitieren werde. Danke für die Weiterentwicklung, die ich sowohl in wissenschaftlicher Hinsicht als auch in sozialer als Mitglied deines Teams machen durfte. Danke für das Vertrauen, das Du in mich hast.

Next, I want to thank all my colleagues in the Institute of Stroke and Dementia Research, especially all group members of AG Liesz who created a very supportive environment. I am grateful for every minute I had the possibility to work with you. Your scientific knowledge and passion about science was inspiring. Especially Stefan Roth and Rebecca Sadler were not only open for every discussion but also became good friends. And I am very grateful for all the motivational coffee breaks with Rainer Malik. I also want to give a special thanks to Benno Gesierich and Marco Düring for not only collaborating on this exciting project but also gently and patiently advising and teaching me. Another special thanks to Prof. Dr. Martin Dichgans for the possibility to work in the Institute for Stroke and Dementia Research. And big thank you is for my flat mate Franz Hell with whom I had endless fruitful discussions on both neuro- and data science.

Zuletzt möchte ich meinen besten Freunden Felicitas Heinen und Leisa Schlösser danken. Danke für euere treue Begleitung durch diese herausfordernde Zeit.